Biophysical Journal Volume 74 March 1998 1115–1134

Loss of Conformational Stability in Calmodulin upon Methionine Oxidation

Jun Gao,* Daniel H. Yin,* Yihong Yao,* Hongye Sun,* Zhihai Qin,* Christian Schöneich,# Todd D. Williams,§ and Thomas C. Squier*

*Departments of Biochemistry, Cell, and Molecular Biology; #Pharmaceutical Chemistry; and §Mass Spectrometry Laboratory, University of Kansas, Lawrence, Kansas 66045-2106 USA

ABSTRACT We have used electrospray ionization mass spectrometry (ESI-MS), circular dichroism (CD), and fluorescence spectroscopy to investigate the secondary and tertiary structural consequences that result from oxidative modification of methionine residues in wheat germ calmodulin (CaM), and prevent activation of the plasma membrane Ca-ATPase. Using ESI-MS, we have measured rates of modification and molecular mass distributions of oxidatively modified CaM species (CaM_{ox}) resulting from exposure to H_2O_2. From these rates, we find that oxidative modification of methionine to the corresponding methionine sulfoxide does not predispose CaM to further oxidative modification. These results indicate that methionine oxidation results in no large-scale alterations in the tertiary structure of CaM_{ox}, because the rates of oxidative modification of individual methionines are directly related to their solvent exposure. Likewise, CD measurements indicate that methionine oxidation results in little change in the apparent α-helical content at 28°C, and only a small (0.3 ± 0.1 kcal mol^{-1}) decrease in thermal stability, suggesting the disruption of a limited number of specific noncovalent interactions. Fluorescence lifetime, anisotropy, and quenching measurements of *N*-(1-pyrenyl)-maleimide (PMal) covalently bound to Cys^{26} indicate local structural changes around PMal in the amino-terminal domain in response to oxidative modification of methionine residues in the carboxyl-terminal domain. Because the opposing globular domains remain spatially distant in both native and oxidatively modified CaM, the oxidative modification of methionines in the carboxyl-terminal domain are suggested to modify the conformation of the amino-terminal domain through alterations in the structural features involving the interdomain central helix. The structural basis for the linkage between oxidative modification and these global conformational changes is discussed in terms of possible alterations in specific noncovalent interactions that have previously been suggested to stabilize the central helix in CaM.

INTRODUCTION

Oxidative damage to a range of proteins correlates with the loss of calcium homeostasis in a wide variety of diseases, including cancer, ischemia, Alzheimer's and Parkinson's disease, amyotrophic lateral sclerosis, and normal biological aging (Fliss and Docherty, 1987; Harman, 1987; Coyle and Puttfarcken, 1993; Rosen et al., 1993; Alexianu et al., 1994; Smith et al., 1996; Sohal and Weindruch, 1996). A possible mechanistic link between oxidative damage of specific calcium regulatory proteins and the loss of calcium regulation associated with these diseases has been suggested (Khachaturian, 1994; Selkoe, 1997). In support of this hypothesis, we have previously identified the in vivo oxidative modification of multiple methionines to their corresponding sulfoxides in calmodulin (CaM) isolated from the brains of aged Fischer 344 rats (Michaelis et al., 1996). There were no detectable oxidative modifications to any amino acids except methionine. Similarly, in vitro oxidation with either hydrogen peroxide (H_2O_2) or peroxynitrite ($ONOO^-$) results in the selective oxidative modification of multiple methionines to methionine sulfoxide (Yin et al., 1995; Yao et al., 1996; Hühmer et al., 1996; Michaelis et al., 1996). Regardless of whether CaM is isolated from aged brain or subjected to in vitro oxidative modification, oxidatively modified calmodulin (CaM_{ox}) acts as an inhibitor with respect to the activation of the plasma membrane (PM) Ca-ATPase by native CaM (Yin et al., 1995; Yao et al., 1996). Therefore, the formation of methionine sulfoxide disrupts some, but not all, specific interactions between CaM_{ox} and the PM-Ca-ATPase that are normally involved in enzyme activation. Because the PM-Ca-ATPase is the major high-affinity, high-capacity transport system present in all cells (Carafoli, 1987; James et al., 1995), the oxidative modification of methionines in CaM has the potential to alter intracellular calcium levels.

An understanding of the structural effects associated with the oxidative modification of specific methionines to their corresponding methionine sulfoxides is complicated by the difficulty of obtaining a homogeneous sample in which individual methionines are selectively oxidized. Separation methods for isolating individual monooxidized species have been unsuccessful because methionine sulfoxide formation in CaM results in 1) no change in net charge, 2) only small changes in calcium affinity, and 3) subtle changes in the secondary and tertiary structure of CaM. Likewise, it has not been possible to simulate structural changes in CaM_{ox}

Received for publication 28 February 1997 and in final form 20 November 1997.

Address reprint requests to Dr. Thomas C. Squier, Department of Biochemistry, Cell and Molecular Biology, University of Kansas, Lawrence, KS 66045-2106. Tel.: 785-864-4008; Fax: 785-864-5321; E-mail: tcsquier@kuhub.cc.ukans.edu.

0006-3495/98/03/1115/20 $2.00

through the use of standard methods of site-directed mutagenesis by substituting individual methionines with naturally occurring amino acids that have a polarity and size similar to those of methionine sulfoxide (e.g., glutamine; Chin and Means, 1996). Therefore, to determine the relationship between methionine oxidation and global structural changes, our strategy has been to use electrospray ionization mass spectrometry to directly measure the average extent of methionine oxidation in CaM and to investigate the relationships between methionine oxidation and alterations in the average structural properties of oxidatively modified CaM, by using circular dichroism (CD) and fluorescence spectroscopy. Whereas CD measurements permit the detection of possible changes in secondary structure associated with the formation of methionine sulfoxide in CaM_{ox}, complementary measurements associated with fluorescence signals from PMal covalently bound to the single cysteine (i.e., Cys^{26}; see Fig. 1) in calcium binding loop I permit the measurement of 1) the average structural features and 2) the fraction of CaM that is structurally perturbed (f_{ox}) around Cys^{26} in the amino-terminal domain of CaM_{ox}. We find that although oxidative modification of a limited number of methionines results in minimal alterations in the secondary structural features of CaM_{ox}, there is a small decrease in the thermal stability of CaM_{ox} relative to native CaM. Large alterations in the lifetime properties of PMal covalently bound to Cys^{26} upon methionine oxidation suggest that methionine oxidation in the carboxyl-terminal domain results in global structural changes involving the amino-terminal domain around Cys^{26}. Because there are no large changes in the average spatial separation between the opposing globular domains of CaM, these results indicate that concerted structural changes within the amino-terminal domain that result from the oxidative modification of methionines in the carboxyl-terminal domain probably involve the interdomain central helix. These results suggest that oxidative modification of selected methionines in CaM_{ox} disrupt specific noncovalent interactions that normally stabilize the structure of native CaM.

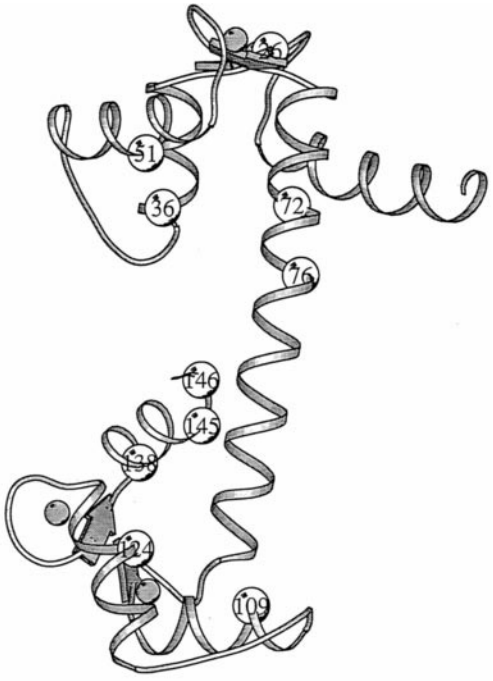

FIGURE 1 Ribbon drawing depicting the backbone fold of calcium-saturated CaM. The relative positions of Cys^{26}, Tyr^{138}, and the eight methionines in wheat germ CaM are indicated. Ribbons represent the protein backbone of CaM, and shaded circles represent calcium ligands. The rate of oxidative modification associated with individual methionines has previously been shown to correlate with the calculated surface accessibilities of the individual sulfur atoms in specific tryptic fragments (Yao et al., 1996), which correspond to the following normalized distribution: Met^{36} (8 ± 2%), Met^{51} (14 ± 4%), Met^{72} (9 ± 2%), Met^{76} (12 ± 17%), Met^{109} (3 ± 4%), Met^{124} (8 ± 1%), and Met^{145} (20 ± 6%), and Met^{146} (27 ± 11%). The numbering of the amino acids in the wheat germ sequence differs by one from a previous report (Yao et al., 1996), and reflects the correction of the original sequence associated with the amino-terminal tryptic fragment as discussed in the text. Coordinates are taken from Brookhaven Protein Data Bank file 1cll.pdb, which corresponds to the human isoform of CaM (Chattopadhyaya et al., 1992). The illustration was created using MolScript (Kraulis, 1991), and assumes that the relative positions of the individual amino acids in wheat germ assume the same backbone structure. The model does not attempt to depict known alterations in the tertiary structure that occur in solution (Heidorn and Trewhella, 1988; Bayley and Martin, 1992; Török et al., 1992; Yao et al., 1994; Finn et al., 1995; reviewed by Crivici and Ikura, 1995).

MATERIALS AND METHODS

Materials

Hydrogen peroxide (H_2O_2) was obtained from Fisher, and the concentration was determined using the extinction coefficient at 240 nm (Nelson and Kiesow, 1972). *N*-1-(Pyrenyl)maleimide (PMal) was obtained from Molecular Probes (Junction City, OR). Tetranitromethane (TNM) was obtained from Aldrich (Milwaukee, WI). All other chemicals were the purest grade commercially available. Wheat germ CaM was purified as previously described by Strasburg et al. (1988). A single isoform of CaM corresponding to the cDNA encoding vertebrate CaM, provided by Prof. Sam Geoge (Duke University), was subcloned and overexpressed in *Escherichia coli*, and was purified, essentially as previously described, by using phenyl Sepharose CL-4B (Pharmacia, Piscataway, NJ) and weak anion exchange high-performance liquid chromatography (HPLC) (Hühmer et al., 1996). Purified CaM was stored at −70°C.

Site-specific chemical modification of either Cys^{26} or Tyr^{138} in wheat germ CaM

The chemical modification of Cys^{26} with PMal and nitration of Tyr^{138} with TNM were carried out essentially as previously described (Yao et al., 1994). The uniform chemical modification of CaM with PMal routinely involved labeling CaM before its exposure to H_2O_2. Control measurements indicate that PMal is not oxidatively modified by H_2O_2, because the retention time and associated area of the PMal-modified tryptic fragment (i.e., E_{15} to K_{31}) resolved by reversed-phase HPLC was unaffected by the oxidative modification of 1.5 ± 0.1 methionines per CaM (i.e., the exposure of CaM to 5 mM H_2O_2 at pH 5.0 for 10 h at 25°C; data not shown). Likewise, the associated absorption spectrum, fluorescence emission spectrum, excited state lifetime, and solvent accessibility of PMal-CaM were virtually identical whether CaM was labeled with PMal before or after oxidative modification (data not shown), indicating that PMal is not modified by H_2O_2 under these experimental conditions. Similar chromato-

graphic and spectroscopic measurements indicated that Tyr^{138} was not oxidatively modified by H_2O_2 under these experimental conditions. CaM concentration was determined from the micro BCA assay (Pierce), using a stock solution of desalted bovine CaM, whose concentration was obtained using the published extinction coefficient for bovine CaM ($\epsilon_{277} = 3029\ M^{-1}\ cm^{-1}$; Strasburg et al., 1988).

Oxidative modification of selected methionines in CaM

The oxidative modification of wheat germ CaM was carried out as described by Yao et al. (1996). CaM (60 μM) was dissolved in 50 mM homopiperazine- *N,N′*-bis-(ethanesulfonic acid) (pH 5.0), 0.1 M KCl, 1 mM $MgCl_2$, 0.1 mM $CaCl_2$. H_2O_2 was added to make the final concentration 5 mM. The oxidation was carried out at 25°C. At different time intervals, the reaction was terminated by applying the sample to a Sephadex G-25 column (1.6 × 23 cm); CaM was eluted from the unreacted H_2O_2 in the void volume and subsequently lyophilized. From direct chromatographic and mass spectrometric measurements relating to the extent of oxidative modification associated with individual amino acids in CaM, we know that 1) methionines are selectively oxidized to their corresponding sulfoxides; 2) no other amino acids are oxidatively modified to any appreciable extent; and 3) the carboxyl-terminus methionines (i.e., Met^{145} or Met^{146}) in CaM_{ox} are the major sites of oxidative modification and represent more than 45% of the oxidatively modified residues in CaM (Yao et al., 1996).

Mass spectrometry

Mass spectra were obtained with an AUTOSPEC-Q tandem hybrid mass spectrometer (VG Analytical, Manchester, England) equipped with an OPUS data system. FAB mass spectrometry experiments were performed using a cesium gun operated at 20 keV energy and 2 μA emission. Post-HPLC column fractions containing tryptic peptides were collected and dried before being redissolved in equal parts of CH_3CN/H_2O (v/v). To this sample an identical volume of a matrix solution containing equal parts of thioglycerol/glycerol (v/v) was added. Peptide esterifications were carried out by dissolving dried peptide fractions in 0.2 N acetyl chloride in hexanol and warming at 35°C for 1 h. The hexanol peptide solutions were analyzed directly. Mass identification was assisted through the use of software (GPMAW from Lighthouse data, Aalokken 14, DK-5250, Odense SV, Denmark) in combination with sequence data derived from the published sequence of wheat germ CaM (Toda et al., 1985).

Electrospray ionization (ESI) spectra were acquired on the AUTOSPEC-Q equipped with the VG's Mark IV ESI source (Micromass, Manchester, England). This version has "pepper pot" counter-electrode and hexapole transfer optics. Unless otherwise indicated, the instrument was operated in negative ion mode at 4 kV acceleration potential, with the ESI needle at 7.5 kV, the counter-electrode at 5 kV, and the remaining lens optimized for maximum sensitivity, using a solution containing 6 pmole/μl of ubiquitin (Sigma, St. Louis, MO) in a solution containing 70% (v/v) methanol and 0.3% (v/v) NH_4OH. The instrument was tuned to 1800 resolving power and scanned from 800 to 3000 amu at 10 s/decade. Mass calibration was with a CsI solution. CaM samples in 0.1 mM EGTA were trapped and desalted before ESI on a column (10 mm × 1 mm) of polymeric beads with 4000 Å pores (Michrom BioResources, Auburn, CA) with 10 mM $(NH_4)_2CO_3$ (pH 8.6) at 250 μl/min. The trapped CaM was eluted from the beads directly into the ESI source with 70% (v/v) methanol and 10 mM $(NH_4)_2CO_3$ (pH 8.6) at 8 μl/min through a 130-μm ID stainless steel needle and nebulized with a coaxial gas flow of nitrogen at 10 liters/h.

Circular dichroism spectroscopy

Circular dichroism (CD) spectra were measured with an AVIV Model 60DS spectropolarimeter and a temperature-jacketed spectral cell with a pathlength of 0.5 cm. Desalted CaM (50 μg/ml) was dissolved in 10 mM Tris-HCl (pH 7.5), 0.1 M $KClO_4$, 1 mM $Mg(ClO_4)_2$, and 0.1 mM $Ca(ClO_4)_2$, and spectra were recorded at 1-nm intervals between 202 and 260 nm. The apparent α-helical content associated with CaM was determined by a nonlinear least-squares fit to computed basis spectra based on the CD spectra of proteins with known 3-D structures (Saxena and Wetlaufer, 1971), using the Levenberg-Marquardt equation solver in the program Mathcad (Mathsoft, Cambridge, MA) to fit the following equation:

$$\begin{aligned}\text{Atual spectrum} = A_1 \times [\alpha\text{-helix}] + A_2 \times [\beta\text{-sheet}] \\ + A_3 \times [\text{random coil}].\end{aligned} \quad (1)$$

This analysis assumes that the actual spectrum is a linear combination of the spectral intensity associated with the indicated secondary structural elements. A_1, A_2, and A_3 are the relative amplitudes associated with the amount of α-helix, β-sheet, and random coil structures in oxidatively modified or native CaM. Alterations in the free energy associated with the stability of CaM were analyzed using a simple two-state model that assumes a highly cooperative temperature-dependent denaturation of the α-helical content of CaM (Bectel and Schellman, 1987), where

$$\begin{aligned}\Delta\Delta G'_{T_m} &= \Delta G'_{\text{native}} - \Delta G'_{\text{oxidized}} \\ &= -RT_m \ln \frac{[\alpha\text{-helix}_{\text{native}}]_{T_m}}{[\alpha\text{-helix}_{\text{native}}]_{10°C} - [\alpha\text{-helix}_{\text{native}}]_{T_m}}.\end{aligned} \quad (2)$$

$\Delta\Delta G'$ is the loss of free energy in CaM_{ox} relative to native CaM in kcal $mole^{-1}$; T_m is the temperature in °K, where the α-helical content of CaM_{ox} is 50% of that at 10°C; and R is the gas constant.

Fluorescence measurements

Steady-state and frequency-domain fluorescence measurements were made using an ISS K2 fluorometer in conjunction with the 351 line (for the excitation of pyrene) from a Coherent Innova 400 laser, as previously described (Yao et al., 1994), and the fluorescence emission was collected subsequent to passage through a Schott GG400 long-pass filter. In all cases, the sample temperature was 25°C, and the buffer consisted of 0.1 M HEPES (pH 7.5), 0.1 M KCl, 1 mM $MgCl_2$ (Buffer A), and either 0.1 mM $CaCl_2$ or 0.1 mM EGTA.

Resolution of fluorescence lifetime components for oxidatively modified CaM

The intensity decay law of the mixture of oxidatively modified and native CaM is obtained from the frequency response of the amplitude-modulated light and is characterized by the frequency (ω)-dependent values of the phase-shift (ϕ_ω) and the extent of demodulation (m_ω). The measured parameters are compared with the calculated (c) values ($\phi_{c\omega}$ and $m_{c\omega}$), and the reported values are those that minimize the squared deviation. Explicit expressions have been provided that permit the ready calculation of the lifetime components relating to a multiexponential decay (i.e., α_i and τ_i; Weber, 1981; Lakowicz et al., 1985), where

$$\Phi_{c\omega} = \arctan \frac{N_\omega}{D_\omega} \quad \text{and} \quad m_{c\omega} = \sqrt{N_\omega^2 + D_\omega^2}. \quad (3)$$

N_ω and D_ω are specific mathematical transforms that relate the measured phase shift (i.e., ϕ_ω) and modulation (m_ω) to the lifetime components associated with the excited state intensity decay of the chromophore. Alternatively, appropriate expressions have been derived that permit determination of the initial anisotropy in the absence of rotational diffusion (r_o), the rotational correlation times (ϕ_i), and the amplitudes of the total anisotropy loss associated with each rotational correlation time ($r_0 g_i$). The derivation and application of these expressions have previously been

described in detail (Lakowicz et al., 1985; Lakowicz and Gryczynski, 1991; Johnson and Faunt, 1992).

These transforms (i.e., N_ω and D_ω) can be readily modified to take into account a heterogeneous solution of CaM that can be approximated by two populations of structural conformers corresponding to 1) native or oxidatively modified CaM with a native-like structure or 2) oxidatively modified CaM with an altered tertiary structure, where

$$N_{\omega\,i} = f_{\text{oxidized}\,i} \times N_{\text{oxidized}} + (1 - f_{\text{oxidized}\,i}) \times N_{\text{native}} \qquad (4)$$

and

$$D_{\omega\,i} = f_{\text{oxidized}\,i} \times D_{\text{oxidized}} + (1 - f_{\text{oxidized}\,i}) \times D_{\text{native}}. \qquad (5)$$

An independent measurement of the individual lifetime components and associated amplitudes relating to native CaM (i.e., α_i and τ_i) permits one to recover 1) the average lifetime parameters (i.e., α_i and τ_i) associated with the structurally altered population of CaM_{ox} and 2) the associated fraction (i.e., f_{oxidized}) of CaM that has been structurally altered by oxidative modification. It should be emphasized that oxidative modification of a particular methionine in CaM_{ox} need not perturb the structural features around PMal at Cys^{26}, and that some oxidatively modified CaM species may have a "native-like" structure that would not contribute to f_{oxidized}. The parameter values are determined using the method of nonlinear least-squares analysis in which the reduced chi-squared (i.e., χ_R^2) is minimized (Bevington, 1969). A comparison of χ_R^2 provides a quantitative measurement of the adequacy of different assumed models to describe the data (Lakowicz and Gryczynski, 1991). Data were fit using either the Globals software package (University of Illinois, Urbana-Champaign) or the program Mathcad 6.0 (MathSoft). The reported experimental uncertainties associated with each parameter were determined from a global analysis of the respective error surfaces, by using the F statistic associated with one standard deviation (Beechem et al., 1991). To simplify the presentation of the data, in cases where the error surfaces are not symmetrical, the reported errors represent the maximum variance obtained from the error analysis.

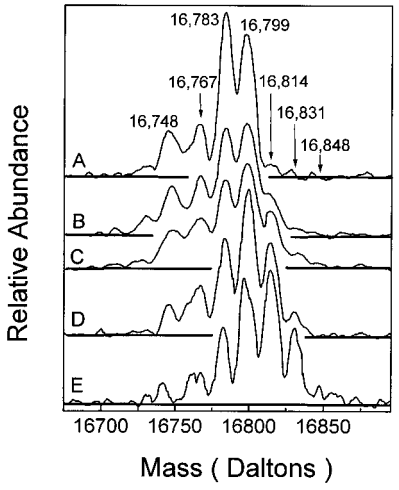

FIGURE 2 ESI MS spectrum of native and oxidatively modified wheat germ CaM after deconvolution of multiply charged ions. Spectra corresponding to native CaM (*A*) or subsequent to exposure with 5 mM H_2O_2 for 1 h (*B*), 2 h (*C*), 4 h (*D*), or 10 h (*E*), using experimental conditions as described in Materials and Methods. Two CaM isoforms were resolved with masses of 16,783 ± 3 and 16,799 ± 3 Da. Cone fragments corresponding to these two CaM isoforms result in two additional species with masses of 16,748 ± 3 and 16,767 ± 3 Da, respectively. The theoretical average molecular mass of wheat germ CaM directly determined from the amino acid sequence and deduced from cDNA analysis was 16,799.6 and 16,785.5 Da, respectively (Toda et al., 1985, 1994; Yang et al., 1996). Subsequent to oxidative modification, the fraction of CaM species containing zero, one, two, and three incorporated oxygens was resolved using ESI MS, and after correction for cone fragmentation and deconvolution of the overlapping oxiforms associated with the two CaM isoforms, the associated fractions of each of these species were tabulated (Table 2). Experimentally, 15 μg of CaM in 0.1 mM EGTA and 10 mM $(NH_4)_2CO_3$ (pH 8.6) was trapped, desalted, and then directly infused (on-line) into an Autospec EQ mass spectrometer, as described in Materials and Methods.

RESULTS

Identification of multiple isoforms of CaM expressed in wheat germ

To identify the distribution of oxiforms of CaM produced under various oxidation conditions, we have made use of the ability of ESI mass spectrometry to resolve the molecular mass of CaM to within 3 Da. We have initially measured the molecular mass of native (unoxidized) CaM to determine the identity of the CaM species purified from wheat germ, because there is some uncertainty with respect to the isoform(s) of CaM expressed in wheat germ. All three of the cDNA derived amino acid sequences expressed in wheat root tip, with calculated average molecular masses of 16,785.5 Da, 16,757.5 Da, and 16,068.0 Da (Yang et al., 1996), are distinct from the reported protein sequence obtained directly from CaM isolated from wheat germ, which has a calculated average molecular mass of 16,799.6 Da (Toda et al., 1985, 1994). It is therefore possible that CaM is differentially expressed in root tip and wheat germ. Alternatively, there may be an error in one of the reported sequences. To identify expressed isoform(s) of CaM in wheat germ, we have used ESI mass spectrometry. The ESI mass spectrum of wheat germ CaM exhibits two major peaks (Fig. 2) with molecular masses corresponding to the mass of wheat germ CaM previously described from its protein sequence (i.e., 16,799 ± 3 Da; Toda et al., 1985, 1994) and to one of the isoforms obtained from an analysis of the cDNA encoding CaM (i.e., 16,783 ± 3; Yang et al., 1996), suggesting the expression of two isoforms of CaM in wheat germ.

Two additional lower molecular masses are observed in the ESI spectrum of native CaM (i.e., 16,748 ± 3 and 16,767 ± 3 Da) that are inconsistent with any of the reported amino acid sequences deduced from the cDNA encoding wheat CaM, suggesting that these masses either 1) correspond to different isoforms of CaM that have previously not been identified or 2) represent fragmentation artifacts that may arise as a result of collision-induced dissociation (CID) (Smith et al., 1991). To investigate the origin of these low mass features in the electrospray ionization mass spectrometry (ESI-MS) spectrum of wheat germ CaM, we have investigated the ESI-MS spectrum of a single isoform of CaM that was cloned and expressed in *E. coli*, and purified to homogeneity by weak-anion exchange HPLC. The single sequence of CaM rules out the possibility that any low-mass features in the spectrum will correspond to isoforms that may be present in CaM isolated from native systems. When the voltage difference across the sampling

orifices in the ESI source is small (i.e., 0 V, low CID energy), we observe two peaks in the ESI-MS spectrum that correspond to average molecular masses of 16,690 ± 3 and 16,706 ± 3 Da, and account for ~11% and 89% of the peak area in the ESI-MS spectrum (Fig. 3 *A*). The major peak (i.e., 16,706 Da) is close to the theoretical mass of the cloned CaM (i.e., 16,705.4 Da). Upon increasing the voltage difference (i.e., 2000 V, high CID energy), the relative area of the 16,690-Da peak increases by approximately twofold, and accounts for 23% of the total peak area in the ESI-MS spectrum (Fig. 3 *B*). In contrast, ESI-MS spectra obtained in positive ion mode (where the spectrum is dominated by ions of lower charge states) contain very little of the 16,690-Da peak, and are dominated by the major peak at 16,706 Da (data not shown). The ability to alter the abundance of the lower mass peak at 16,690 Da by altering the experimental conditions in the mass spectrometer indicates that the 16,690-Da peak represents the mass of a collision-induced dissociation (CID) artifact that results from the conditions used in the electospray ionization, and may correspond to the loss of neutral NH_3 or H_2O. Differences in the relative abundance of this low-mass feature observed in negative and positive ion mode, where the distributions of charge states are very different, is consistent with earlier suggestions that the fragmentation of proteins may be affected by the distribution of charge states, and that there is a reduced fragmentation as a result of the lower collision cross section for a sample populated by ions of a lower charge state (Chen et al., 1997). However, whereas positive ion mode results in less collision-induced cone fragmentation, negative ion mode has been used to resolve the distribution of oxidatively modified CaM species (see below), as a result of the greatly improved experimental sensitivity of CaM observed in negative ion mode. Therefore, the low-mass ions observed in the ESI spectra of wheat germ CaM (i.e., 16,748 Da and 16,767 Da; Fig. 2) are probably also MS collision-induced ionization species. The larger mass difference between the parent ions (i.e., 16,783 Da and 16,799 Da) and their respective fragmentation ions (i.e., 16,748 and 16,767 Da) in CaM isolated from wheat germ relative to that expressed in *E. coli* may be related to the trimethyl-lysine (which is expected to readily fragment in negative mode to loose one methyl group; Murphy and Harrison, 1994) and other sequence differences between wheat germ and vertebrate CaM expressed in *E. coli*.

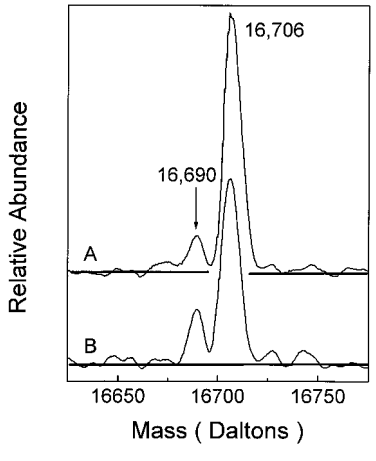

FIGURE 3 Identification of cone fragmentation in the ESI MS spectrum of expressed vertebrate CaM. Spectra of a single isoform of CaM expressed in *E. coli* were measured by using two electrospray needle voltages corresponding to 0 V (*A*) and 200 V (*B*). Experimentally, 15 μg of CaM in 0.1 mM EGTA and 10 mM $(NH_4)_2CO_3$ (pH 8.6) was trapped, desalted, and then directly infused (on-line) into an Autospec EQ mass spectrometer, as described in Materials and Methods.

As already indicated, the two major peaks observed in the ESI mass spectrum (Fig. 2 *A*) are consistent with the presence of two isoforms of CaM expressed in wheat germ (see above). It is also possible, however, that only one isoform of CaM is expressed, and that the larger molecular mass corresponds to that of native CaM that has been oxidatively modified (i.e., 16,783 + 16 = 16,799 Da). To further clarify the origin of these two major peaks in the ESI mass spectrum, we have proteolytically digested wheat germ CaM and used reversed-phase HPLC and fast atom bombardment mass spectrometry (FAB-MS) to identify the resulting tryptic peptides. It should be noted that we have previously identified the masses associated with all but one of the major tryptic fragments (i.e., those peptides containing two or more amino acids) obtained from wheat germ CaM by FAB mass spectrometry (Yao et al., 1996). However, we had been unable to detect a peptide mass that would correspond to the 14 amino acid amino-terminal tryptic fragment (i.e., Ala^1 to Lys^{14}), based on the sequence currently reported in the protein data base, which had a predicted monoisotopic mass of 1662.8 Da (Toda et al., 1985). This sequence has recently been corrected, and is reported to contain 13 amino acids with an expected monoisotopic molecular mass of 1549.7 (Toda et al., 1994).

Using FAB-MS, we find two major tryptic fragments with monoisotopic masses $[M + H]^+$ of 1535.8 ± 0.3 and 1549.8 ± 0.3 Da (Fig. 4 *A*), which correspond to the predicted molecular masses of the amino-terminal tryptic peptides derived respectively from either the direct protein sequence or from that derived from cDNA (Toda et al., 1994; Yang et al., 1996). The calculated monoisotopic molecular masses derived from the sequence data are 1535.6 and 1549.7 Da, respectively. Whereas the 1549.7-Da mass had previously been reported using FAB-MS (Toda et al., 1994), the 1535.6-Da mass had only been suggested from the cDNA-derived sequence obtained from root tip, and this CaM isoform may not necessarily be expressed in wheat germ. To further clarify the identity of the 1535.8-Da peptide, we have isolated this peptide (Fig. 4 *B*) and derivatized the associated carboxylic acids with hexan-1-ol (which adds 84.0 Da to each carboxylic acid on the parent peptide) and used FAB mass spectrometry to measure the distribution of masses in the resulting products (Fig. 4 *C*). There are four products with monoisotopic masses $[M + H^+]$ of 1620.1 ± 0.3 Da, 1704.0 ± 0.3 Da, 1787.8 ± 0.3 Da, and 1871.6 ± 0.3 Da. Because the conditions used to derivatize this pep-

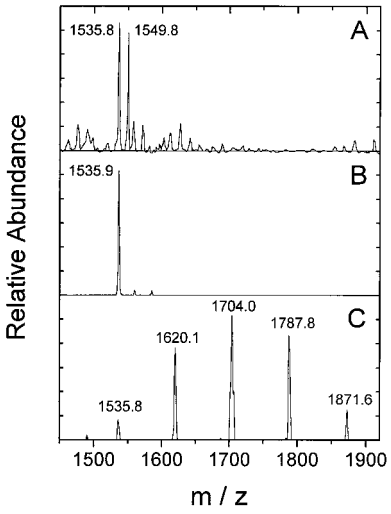

FIGURE 4 FAB mass spectrometric identification of amino-terminal tryptic fragment containing amino acids Ala^1 to Lys^{13}. A tryptic fragment with a retention time of 31.8 min on a Vydac C4 reversed-phase column employing a linear gradient varying from 0.1% TFA to 0.1% TFA in 80% acetonitrile/20% water at a rate of 1%/min was collected as previously described (Yao et al., 1996) and was introduced directly into the mass spectrometer (*A*). After the chromatographic separation of the 1536 Da peptide (*B*), carboxylic groups were esterified with hexan-1-ol in hydrochloric acid (*C*). FAB experiments and peptide esterifications were performed as described in Materials and Methods.

TABLE 1 Comparison of N-terminal sequences from higher plants with vertebrate CaM

ADQLTDEQIAEFK[a]	*Triticum aestivum* (wheat)*
------D------[b]	*Triticum aestivum* (wheat)[#]
----------[c]	*Zea mays* (corn)[#]
------D-T----[d]	*Zea mays* (corn)[#]
-E---E-------[e]	*Solanum tuberosum* (potato)[#]
-----ED--S---[f]	*Solanum tuberosum* (potato)[#]
------D--S---[g]	*Brassica juncea* (leaf mustard)[#]
------D------[h]	*Hordeum vulgare* (barley)[#]
------D--S---[i]	*Bryonia dioica* (red bryony)[#]
???----------[j]	*Spinacia oleracea* (spinach)*
-----E-------[k]	*Bovine* (cow)*

[a]Toda et al., 1985; Toda et al., 1994; [b]Yang et al., 1996; [c]Griess et al., 1994; [d]Breton et al., 1995; [e]Jena et al., 1989; [f]Takezawa et al., 1995; [g]Chye et al., 1995; [h]Ling and Zielinski 1989; [i]Galaud et al., 1993; [j]Lukas et al., 1984; [k]Grand and Perry, 1978. *Protein sequence directly determined. [#]Protein sequence derived from cDNA.

tide are not expected to quantitatively modify all four carboxylic groups, a distribution of masses is expected that corresponds to various levels of derivatization. These results are consistent with the presence of the four reported carboxylic acids in the amino-terminal tryptic fragment that had been suggested from the cDNA-derived sequence (Yang et al., 1996).

Thus the two major peaks observed in the ESI mass spectrum (Fig. 2 *A*) correspond to two isoforms of CaM expressed in wheat germ that differ in the sequence of their amino-terminal tryptic fragment. Both sequences contain 13 amino acids and differ in the substitution of either of Asp^7 or Glu^7 (i.e., ADQLTDD_7QIAEFK or ADQLTDE_7QIAEFK). Similar sequence differences in this amino acid position have previously been reported in cDNA-derived sequences for multiple isoforms of CaM present in a range of different higher plants (Table 1). Thus multiple isoforms of CaM that contain both sequences have been reported in corn, potato, and wheat (Jena et al., 1989; Griess et al., 1994; Toda et al., 1994; Breton et al., 1995; Takezawa et al., 1995; Yang et al., 1996), whereas cDNA-derived CaM isoforms that contain only Glu^7 (spinach) or Asp^7 (barley, leaf mustard, and red bryony) provide further support that there is a large amount of heterogeneity with respect to the identity of the acidic amino acid at this position encoded within the DNA sequences for plant CaM (Ling and Zielinski, 1989; Galaud et al., 1993; Chye et al., 1995). Our results provide strong support that two isoforms of CaM containing both sequences are expressed in wheat germ in approximately equal abundances. Both sequences fully activate a range of different target proteins, as evidenced by the equivalent levels of activation in comparison with that of vertebrate CaM (Strasburg et al., 1988; Yao et al., 1994), suggesting that the conservative substitution of Asp for Glu results in minimal differences in the tertiary structure of CaM.

Mass spectrometric resolution of the distribution of oxidatively modified CaM_{ox}

Previous results obtained using reversed-phase HPLC and FAB-MS to separate and identify the tryptic peptides obtained from native or oxidatively modified wheat germ CaM permitted an estimate of the average extent of oxidative modification associated with specific methionines within the primary sequence of wheat germ CaM (Yao et al., 1996). These measurements provided no information regarding the number of oxygens incorporated into each CaM molecule, and could not distinguish between the random oxidative modification of methionines located on different CaMs from the presence of a small population of CaM molecules containing multiple methionine sulfoxides coexisting with a larger population of unmodified CaMs. However, because we have previously shown that the rate of oxidation of individual methionines is directly related to their solvent accessibilities (Yao et al., 1996), it is possible that structural changes induced by the oxidative modification of one methionine may enhance the susceptibility of other methionines in the same polypeptide chain to further oxidative modification, resulting in the preferential oxidative modification of multiple methionines located on the same CaM. To investigate this possibility, we have used electrospray mass spectrometry (ESI-MS) to directly measure the fraction of CaM molecules containing zero, one, two, three, or more incorporated oxygens in CaM samples with variable levels of oxidative modification.

There are two isoforms of native wheat germ CaM with molecular masses of 16,783 ± 3 Da (isoform 1) and 16,799 Da (isoform 2; see above). Upon oxidation with H_2O_2, additional species with average masses of 16,814 ± 3 Da,

16,831 ± 3 Da, and 16,848 ± 3 Da appear (Fig. 2); these species having 16 ± 1 amu differences are consistent with the oxidative modification of one, two, and three methionines, respectively. There are no CaM species with molecular masses greater than 16,848 Da, indicating that oxidative modification of CaM is limited to the oxidation of, at most, four methionines in any single CaM after exposure to 5 mM H_2O_2 for 10 h.

The area of each peak in the ESI-MS spectra provides an estimate of the relative abundance of each CaM species. However, quantitation of the relative amount of the different CaM oxiforms (populations of CaM species containing a specific integral number of incorporated oxygens) is complicated by 1) the ESI-induced fragmentation of CaM (see above) and 2) the presence of two CaM isoforms that differ in molecular mass by 14 Da, resulting in the superposition of the oxidation products of Isoform 1 [$CaM(O)_n$] with those of Isoform 2 [$CaM(O)_{n-1}$]. Because for native CaM the areas associated with the fragmentation peaks at 16,748 and 16,767 Da represent 28% of the total area of the ESI-MS spectrum (Fig. 2 *A*), the observed area of any particular peak in the ESI-MS spectrum can be corrected for fragmentation artifacts by using the following algorithm:

$$\text{Corr. area}_{CaM(O)_n} = [\text{Obs. area}_{CaM(O)_n} - [0.4 \times \text{Obs. area}_{CaM(O)_{n+2}}]] \times 1.4,$$

which corrects for 1) the loss of spectral intensity resulting from fragmentation of a particular oxiform of CaM [i.e., $CaM(O)_n$] and 2) the increased peak intensity resulting from the collision-induced fragmentation of a more highly oxidized species [$CaM(O)_{n+2}$] whose fragmentation products overlap with the species of interest [$CaM(O)_n$]. Separation of the various oxiforms of both isoforms of CaM is possible if one remembers that the methionines in both isoforms 1 and 2 are equivalent, and are expected to have the same sensitivity to oxidative modification by H_2O_2. Therefore, it is reasonable to assume that the highest mass peak in the ESI-MS spectrum corresponds to the most highly oxidized population of isoform 2, and contains very little isoform 1.

Knowing that ESI-induced fragmentation results in a 28% decrease in the associated area, the corrected peak area associated with the 16,848-Da peak (which contains 6% of the total spectral intensity after 10 h of oxidation with H_2O_2; Fig. 2 *E*) represents 8% of the total area, and corresponds to an oxiform of isoform 2 with three oxidized methionines [i.e., $CaM_2(O)_3$]. Because isoform 1 should have the same population of CaM oxiforms, 8% of the corrected ESI-MS peak area of the 16,831-Da peak (which comprises 17% of the total ESI-MS peak area, after correction for ESI-induced fragmentation) represents an oxiform of isoform 1 with three oxidized methionines [i.e., $CaM_1(O)_3$]. The remainder (i.e., 9% of the total area) corresponds to isoform 2 [i.e., $CaM_2(O)_2$]. Likewise, the peak at 16,814 Da (which comprises 42% of the total ESI-MS peak area) corresponds to a mixture of isoforms 1 and 2, in which ~9% of the total ESI-MS peak area corresponds to isoform 1 [i.e., $CaM_1(O)_2$] and the remainder (i.e., ~33% of the total area) corresponds to isoform 2 [i.e., $CaM_2(O)_1$]. Consequently, the peak at 16,799 Da (which comprises 33% of the total ESI-MS peak area) corresponds entirely to isoform 1 [i.e., $CaM_1(O)_1$], and after correction for ESI-MS fragmentation, there is no native isoform 2 or isoform 1 in this sample.

In this manner, the distribution of oxidatively modified CaM species resulting from exposure of CaM to H_2O_2 for varying times and the average number of oxygens incorporated into each CaM sample were calculated (Table 2). After 1, 2, 4, and 10 h of exposure to H_2O_2, an average of 0.40 ± 0.03, 0.58 ± 0.05, 0.72 ± 0.06, and 1.5 ± 0.1 methionines are oxidized to their corresponding methionine sulfoxides in each CaM. These numbers are in reasonable agreement with earlier estimates regarding the amount of methionine oxidation, based on a consideration of alterations in the relative areas associated with the tryptic peptides resolved by reversed-phase HPLC, which suggested that ~1.3 ± 0.1 methionines are oxidatively modified to the corresponding methionine sulfoxide after 10 h of exposure to H_2O_2 (Yao et al., 1996). The general agreement between these complementary measurements provides further confidence in the calculated distributions of oxidatively modified CaM species, and suggests that we can use these samples to investigate possible relationships between methionine oxidation and alterations in the secondary and tertiary structures of CaM_{ox}.

The preponderance of CaM species containing one or two methionine sulfoxides, and the absence of CaM species with more than two methionine sulfoxides in all but the most highly oxidized samples (i.e., CaM exposed to H_2O_2 for 10 h; Table 2), suggest that the oxidative modification of a single methionine to the corresponding methionine sulfoxide does not result in a significant increase in the susceptibility of additional methionines to oxidative modification. Because the rate of oxidative modification of individual methionines in CaM by H_2O_2 is directly related to the solvent accessibility of the individual sulfurs (Yao et al., 1996), these results indicate that oxidative modification of individual methionines in CaM does not result in any large increase in the surface accessibility of other methionines that would predispose them to oxidative modification. Thus methionine sulfoxide formation is not accompanied by any large-scale unfolding or alteration in the tertiary structure of either the amino- or carboxyl-terminal domains in CaM_{ox}.

Additional information regarding possible alterations in the susceptibility of individual methionines to oxidative modification is provided by a quantitative consideration of the distribution of CaM oxiforms observed in the ESI mass spectra subsequent to the modification of a variable number of methionines. This analysis provides information regarding the specificity of oxidative modification and of the optimal choice of experimental conditions that minimize the modification of multiple methionines in each CaM (Fig. 5). The data were simultaneously fit by using the method of nonlinear least squares to a series of second-order rate equations involving the following model:

TABLE 2 Distribution of CaM species after oxidative modification with H_2O_2[a]

Mass (Da)	Native	1 h	2 h	4 h	10 h
16,783					
Isoform 1 (0 oxygen)	49%	36%	29%	18%	0%
Isoform 2 (NA)	0%	0%	0%	0%	0%
Total area	49%	36%	29%	18%	0%
16,799					
Isoform 1 (1 oxygen)	0%	12%	17%	22%	33%
Isoform 2 (0 oxygen)	51%	32%	25%	24%	0%
Total area	51%	44%	42%	46%	33%
16,814					
Isoform 1 (2 oxygen)	0%	4%	6%	7%	9%
Isoform 2 (1 oxygen)	0%	12%	17%	22%	33%
Total area	0%	16%	23%	29%	42%
16,831					
Isoform 1 (3 oxygen)	0%	0%	0%	0%	8%
Isoform 2 (2 oxygen)	0%	4%	6%	7%	9%
Total area	0%	4%	6%	7%	17%
16,848					
Isoform 1 (4 oxygen)	0%	0%	0%	0%	0%
Isoform 2 (3 oxygen)	0%	0%	0%	0%	8%
Total area	0%	0%	0%	0%	8%
Distribution of oxiforms					
Native CaM	100%	68 ± 7%	54 ± 6%	42 ± 4%	0%
One oxygen	0%	24 ± 2%	34 ± 4%	44 ± 5%	66 ± 7%
Two oxygens	0%	8 ± 1%	12 ± 1%	14 ± 2%	18 ± 2%
Three oxygens	0%	0%	0%	0%	16 ± 2%
Fraction of CaM oxidized	0%	32 ± 7%	46 ± 6%	58 ± 4%	100%
Oxygens incorporated/CaM	0	0.40 ± 0.03[b]	0.58 ± 0.05[b]	0.72 ± 0.06[b]	1.5 ± 0.1[b]
Oxygens incorporated/carboxyl-terminus CaM	0	0.30 ± 0.04[c]	0.43 ± 0.06[c]	0.53 ± 0.07[c]	1.1 ± 0.1[c]
Oxygens incorporated/amino-terminus of CaM	0	0.10 ± 0.01[c]	0.15 ± 0.02[c]	0.19 ± 0.02[c]	0.4 ± 0.1[c]

[a] Relative concentrations of different CaM species subsequent to correction for cone fragmentation. Average errors associated with the determination of the different oxiforms of CaM were ± 15% of indicated values, and errors were propagated in the calculation of the distribution of oxiforms and average number of oxygens incorporated in each CaM (Bevington, 1969).

[b] The average number of oxygens incorporated per CaM was calculated using the following formula:

$$\frac{\text{Total oxygen}}{\text{CaM}} = \sum_i (\text{CaM}_i \times n_i),$$

where CaM_i represents the fractional contribution of a specific oxiform of CaM_{ox} containing n_i oxygens.

[c] Oxidative modification of methionines located in the carboxyl-terminus of CaM (i.e., Met^{109}, Met^{124}, Met^{145}, and Met^{146}) account for 74 ± 7% of the oxidatively modified methionines, while oxidative modification of methionines located in the amino-terminus of CaM (i.e., Met^{36}, Met^{51}, and Met^{72}) account for 26 ± 2% of the oxidatively modified methionines. Met^{76} is not detectably oxidized (Yao et al., 1996). In all cases errors were propagated (Bevington, 1969).

$$\text{CaM} \overset{k_1}{\rightarrow} \text{CaM(O)}_1 \overset{k_2}{\rightarrow} \text{CaM(O)}_2 \overset{k_3}{\rightarrow} \text{CaM(O)}_3 \overset{k_4}{\rightarrow} \text{CaM(O)}_4.$$

The indicated rate constants (i.e., k_1, k_2, k_3, and k_4) are a weighted average of the individual rate constants associated with the modification of each of the eight different methionines in CaM. The experimental fits are shown (Fig. 5), and the second-order rate constants are $k_1 = 16.0 \times 10^{-3}$ M^{-1} s^{-1}, $k_2 = 8.5 \times 10^{-3}$ M^{-1} s^{-1}, $k_3 = 3.5 \times 10^{-3}$ M^{-1} s^{-1}, and $k_4 \approx 0$. It is apparent that $k_1 > k_2 > k_3 > k_4$, indicating that the oxidative modification of specific methionines does not dramatically increase the surface accessibilities and associated rates of oxidative modification of the sulfurs associated with additional methionines on the same CaM. Furthermore, more than one oxidative modification on each CaM can be minimized by using experimental conditions that result in an average of less than 0.72 ± 0.06 oxidized methionines per mole of CaM (i.e., exposure of CaM to 5 mM H_2O_2 for 4 h or less), where 76% of the modified species of CaM contain a single methionine sulfoxide (Table 2).

Similar secondary structures of native and oxidatively modified CaM

The effects of oxidative modification on the secondary structure of CaM were assessed by CD spectroscopy to estimate the apparent α-helical content of native and modified CaM (Fig. 6). In these experiments, we used conditions that result in an average of 1.5 ± 0.1 moles of methionine sulfoxide/mole of CaM (i.e., exposure of CaM to H_2O_2 for 10 h), where essentially all of the CaM is oxidatively modified (Table 2). The CD spectrum obtained from CaM_{ox} at 28°C is similar to that of native CaM, with only small spectral differences exhibited in the 208-nm region (Fig. 6

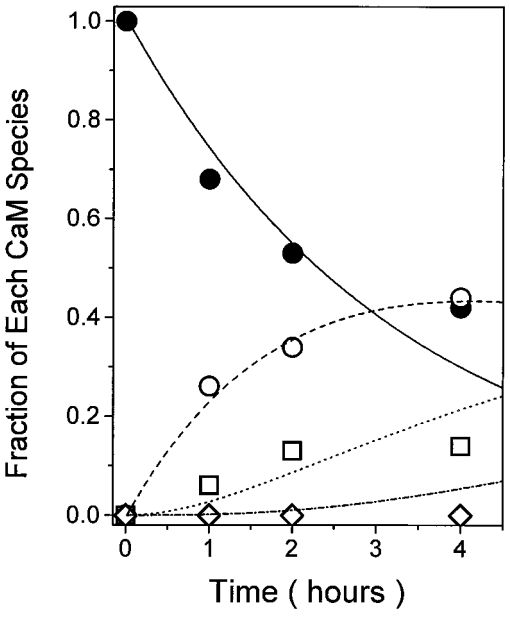

FIGURE 5 Distribution of both native and oxidatively modified oxiforms of CaM. ESI MS spectrometry was used to measure the distribution of CaM species resulting from different degrees of oxidative modification, as documented in Table 2. The fractional contribution of each species of CaM associated with both native CaM (●) and oxidatively modified species containing one additional oxygen (○), two additional oxygens (□), and three additional oxygens (◇) obtained from electrospray mass spectroscopic data is indicated. The experimental fits obtained from the simultaneous fitting of the complete data sets are shown for both native CaM (*solid line*) and for oxidatively modified CaM containing one (*dashed line*), two (*dotted line*), and three (*dash-dotted line*) incorporated oxygens, as described in the text.

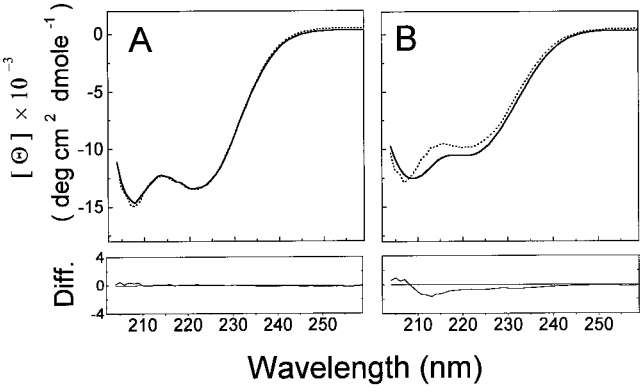

FIGURE 6 Secondary structure of calcium-saturated native and oxidized CaM. CD spectra obtained using native CaM (——) or subsequent to the average oxidative modification of 1.5 ± 0.1 methionines per molecule of CaM (·····) at 28°C (*A*) and 70°C (*B*). The difference spectrum was obtained by subtracting the spectrum associated with native CaM from that of CaM_{ox}. Desalted CaM (50 μg/ml) was dissolved in 10 mM Tris-HCl (pH 7.5), 0.1 M $KClO_4$, 1 mM $Mg(ClO_4)_2$, and 0.1 mM $Ca(ClO_4)_2$. The resulting spectra were analyzed by the method of nonlinear least squares, using Eq. 1 in Materials and Methods. In all cases the errors associated with the experimental determination of the α-helical content of CaM was ~1%. No effort was made to consider systematic errors associated with the calculation of the α-helical content of CaM that may be related to the choice of basis spectra used in fitting the data.

A). This suggests that these samples have similar average secondary structures. These CD spectra were fit to a set of empirical basis spectra characteristic of the secondary structural elements of a range of different proteins (see Eq. 1 in Materials and Methods). Thus, fitting the spectra obtained at 28°C demonstrates that native CaM contains ~58% α-helix, and that there is little difference in the α-helical content of CaM_{ox} relative to native CaM at 28°C (Fig. 6 *A*).

Decreased thermal stability of oxidatively modified CaM

CD spectra associated with native and oxidatively modified CaM were measured at 10° to 15°C intervals between 12° and 90°C (Fig. 7), and the α-helical content was calculated (see above). At 70°C, larger spectral differences are observed in the CD spectra between 202 and 230 nm (Fig. 6 *B*), which correspond to a 19% decrease in the average α-helical content of CaM_{ox} compared to that of native CaM. The estimated half-point of thermal denaturation associated with the secondary structure of native CaM occurs at 97 ± 3° (Fig. 7), whereas that for CaM_{ox} occurs at 87 ± 3°C. The 10° ± 4°C decrease in thermal stability in CaM_{ox} relative to native CaM indicates that methionine sulfoxide disrupts stabilizing interactions between protein structural elements that are important in defining the native structure of CaM. A simple two-state model that assumes a highly cooperative temperature-dependent denaturation of the α-helices in CaM permits the calculation of the destabilization of the native structure associated with CaM_{ox}, and suggests that the oxidative modification of selected methionines results in a 0.3 ± 0.1 kcal mol^{-1} loss in free energy (see Eq. 2 in Materials and Methods). The small decrease in free energy is consistent with the loss of a limited number of noncova-

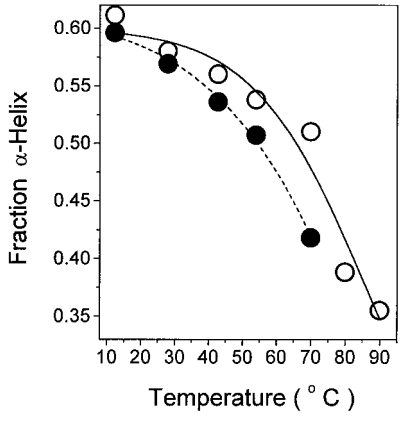

FIGURE 7 Decreased thermal stability upon oxidative modification of methionine in CaM. Temperature dependence of the apparent α-helical content associated with native CaM (○) and subsequent to the oxidative modification of an average of 1.5 ± 0.1 methionines per molecule of CaM (●). The apparent α-helical content was calculated as described in Materials and Methods (see Eq. 1). Sample conditions are as described in legend to Fig. 6.

lent interactions, such as that those involving hydrogen bonding or the formation of specific ion pairs (Alber, 1989; Ehrhardt et al., 1996).

Structural changes in the amino-terminal domain of CaM correlate with the total extent of methionine oxidation

The excited state lifetime of a fluorophore provides a sensitive measurement of its environment within the protein, and is commonly used to monitor structural changes in proteins (Schöneich et al., 1995). To assess specific structural changes in the amino-terminal globular domain of CaM_{ox} that result from methionine oxidation, we measured the frequency response of pyrene maleimide (PMal) covalently bound to Cys^{26} in both native CaM and after oxidative modification by H_2O_2. Upon oxidative modification of a progressively larger number of methionines (i.e., 0.40 ± 0.03, 0.58 ± 0.05, and 0.72 ± 0.06 moles of methionine/mole of CaM; see Table 2), a progressively larger shift was observed in the frequency response of both calcium-saturated and apo-PMal-CaM toward higher frequencies (Fig. 8, *A* and *B*), indicating that the average excited state lifetime of PMal becomes smaller. These large shifts in the frequency response of PMal upon oxidative modification indicate that there are substantial changes in the environment surrounding Cys^{26} associated with methionine sulfoxide formation. These structural changes cannot be explained as the result of any alteration in calcium binding, because direct measurements have previously shown that native and oxidatively modified CaM bind 4.07 ± 0.05 and 3.9 ± 0.2 moles of calcium/mole of CaM, respectively (Yao et al., 1996). Furthermore, the extent of the calcium-dependent shift in the frequency response of PMal-CaM toward higher frequencies (shorter lifetimes) is maintained (Fig. 8, *A* and *B*), irrespective of the extent of oxidative modification.

The frequency response of PMal-CaM upon oxidative modification can be fit to a sum of exponentials, as described in Materials and Methods. The intensity decay of native PMal-CaM is best described by three lifetime components, as indicated by the nearly randomly weighted residuals and the lack of improvement in the fit to a four-exponential model (Fig. 9 *A*). In contrast, four lifetime components are necessary to adequately describe the intensity decay of PMal-CaM subsequent to exposure to H_2O_2 for 4 h (Fig. 9 *B*; Table 3). Because the number of lifetime components necessary to describe the fluorescence intensity decay of a chromophore in a protein is related to the structural heterogeneity surrounding the chromophore (Royer, 1993), the increased complexity of the intensity decay associated with PMal upon methionine oxidation indicates that there is a larger amount of conformational heterogeneity in CaM_{ox}.

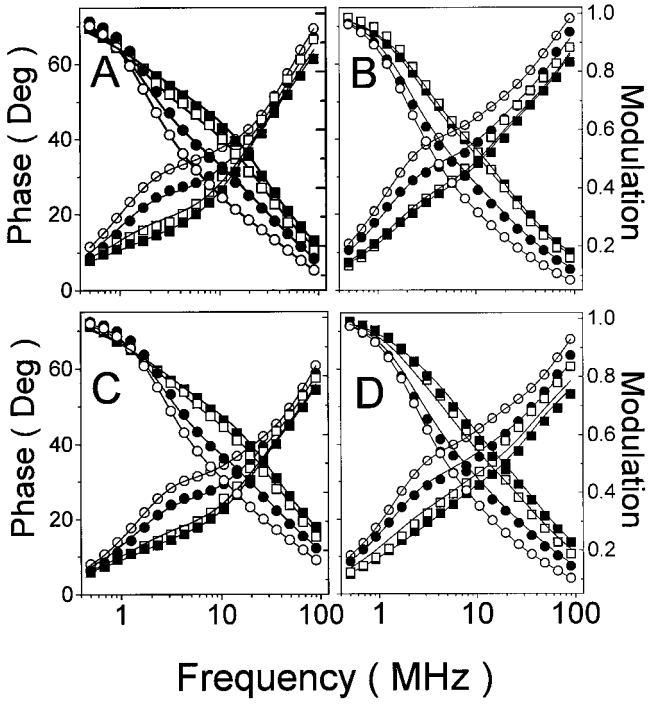

FIGURE 8 Lifetime data for apo- and calcium-activated $PMal_{26}$-CaM in the absence and presence of the fluorescence resonance energy transfer acceptor nitrotyrosine^{138}. Frequency response of phase shift and modulation for PMal bound to Cys^{26} in the absence (*A*, *B*) or presence (*C*, *D*) of the fluorescence resonance energy transfer acceptor nitrotyrosine^{138} for native PMal-CaM (○) and subsequent to the oxidative modification of an average of 0.40 ± 0.03 (●), 0.58 ± 0.05 (□), and 0.72 ± 0.06 (■) methionines per CaM, resulting from the exposure of CaM to H_2O_2 for 1 h, 2 h, and 4 h, as described in Materials and Methods. As the modulation frequency is increased, there is an increasing phase shift and decreasing modulation. Individual data sets in each panel were simultaneously fit to a two-state model, where the fraction of CaM species that are structurally modified around Cys^{26} (i.e., f_{ox}) and the associated average lifetime components (i.e., α_i and τ_i) of the structurally modified population of CaM species were recovered from the fit to the data, as described in Materials and Methods. Experimental conditions involved 1.2 μM CaM in Buffer A and either 0.1 mM $CaCl_2$ (*A*, *C*) or 0.1 mM EGTA (*B*, *D*) at 25°C.

Simultaneous fitting of lifetime data for CaM_{ox} to a two-state model

To obtain additional information regarding the relationships between 1) methionine oxidation, 2) the fraction of oxidized CaM species whose structure is modified (f_{ox}) around Cys^{26}, and 3) the average lifetime parameters, i.e., α_i and τ_i, of PMal in the structurally modified population of CaM_{ox}, three data sets obtained from CaM samples with various extents of oxidative modification (i.e., after exposure to H_2O_2 for 1, 2, and 4 h) were simultaneously fit to a model that assumes that the distribution of species associated with oxidatively modified CaM can be approximated by two structurally different populations, as described in Materials and Methods. The intensity decay of native PMal-CaM was separately fit to a sum of three exponentials (Fig. 9 *A*), and these parameters for native CaM were utilized to determine both f_{ox} and the associated average fluorescence lifetime

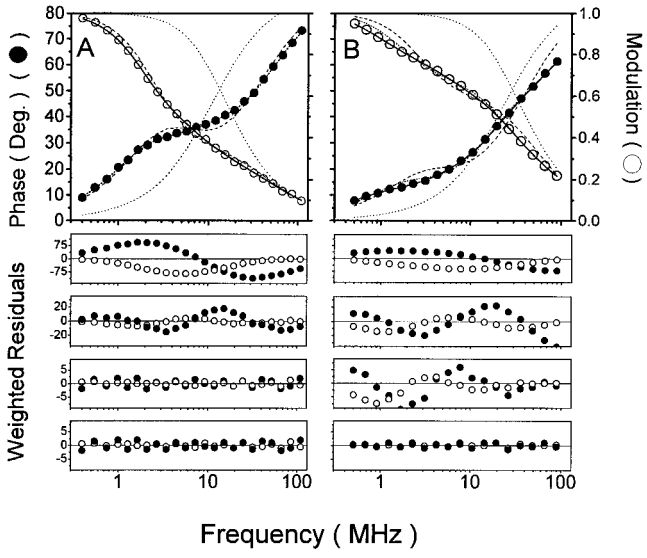

FIGURE 9 Intensity decays of native and oxidatively modified PMal-CaM. Frequency response and multiexponential fits corresponding to the phase shift (●) and modulation (○) for native CaM (*A*) and subsequent to the exposure to 5 mM H_2O_2 for 4 h, which results in the oxidative modification of 0.72 ± 0.06 methionines per CaM (*B*). Data were fit to a sum of exponentials, where

$$I(t) = \sum_i \alpha_i \tau_i .$$

The fits correspond to one (*dotted line*), two (*dashed line*), three (*short dashed line*), and four (*solid line*) exponential components. Weighted residuals are shown below the frequency domain data for the various models, and from top to bottom, correspond to one-, two-, three-, and four-exponential fits to the data. The weighted residuals correspond to the difference between the experimental data and the calculated fit divided by the standard error of the individual measurements, which was assumed to be 0.2° and 0.005 for the phase and modulation data, respectively. Lifetime measurements were made in buffer A in the presence of 0.1 mM $CaCl_2$ at 25°C.

parameters of the CaM_{ox} species that are structurally modified around PMal (Figs. 8 and 10). Just as was observed in fitting the individual intensity decays for PMal-CaM_{ox} (Fig. 9 *B*), the simultaneous fits involving calcium-saturated PMal-CaM containing various levels of oxidative modification require four lifetime parameters to adequately describe the average intensity decay associated with the structurally perturbed population of oxidatively modified CaM, as indicated by the more randomly weighted residuals and the greater than threefold improvement in the χ^R_2 relative to a model involving three lifetime components (Fig. 10). In all cases, the fraction (f_{ox}) of CaM molecules whose structure is modified in samples of oxidatively modified CaM was treated as a floating parameter, and the error surfaces obtained from a nonlinear least-squares global analysis of the data that result in the best fit for calcium saturated PMal-CaM_{ox} are shown in Fig. 11, where $f_{ox}(1\ h) = 0.26 \pm 0.04$, $f_{ox}(2\ h) = 0.54 \pm 0.06$, and $f_{ox}(4\ h) = 0.74 \pm 0.03$. The indicated errors were obtained from the respective error surfaces, and to simplify the tabulation of the experimental parameters, in all cases represent the maximum variance associated with one standard deviation relative to the recovered minimum (because the error surfaces are not necessarily symmetrical around the recovered value of f_{ox}). Similar values of f_{ox} were obtained in the global analysis of both calcium-saturated and apo-PMal-CaM_{ox} in the presence or absence of the fluorescence resonance energy transfer (FRET) acceptor nitrotyrosine[138] (Table 4), and for these four samples the average recovered values correspond to $f_{ox}(1\ h) = 0.26 \pm 0.04$, $f_{ox}(2\ h) = 0.61 \pm 0.10$, and $f_{ox}(4\ h) = 0.78 \pm 0.06$. These recovered values of f_{ox} are similar to the average number of oxygens incorporated into each CaM from ESI-MS (Table 2). Furthermore, f_{ox} is much larger than the extent of oxidative modification associated with the amino-terminus of CaM_{ox}, which has previously been shown to contain only ~25% of the total number of oxidatively modified methionines (Yao et al., 1996). Significantly, it is not possible to obtain a reasonable fit to the fluorescence data shown in Fig. 10 if one assumes that only oxidatively modified methionines located in the amino-terminus of CaM contribute to the structural changes around PMal at Cys^{26} in the amino-terminal domain of CaM. These results strongly indicate that there are structural alterations in the local environment around PMal in CaM_{ox} that result from the oxidative modification of methionines located in the carboxyl-terminal domain, and suggest that the structural coupling between the opposing globular domains in CaM is modified upon oxidative modification.

Increased solvent accessibility of PMal upon oxidative modification of methionine

To better understand the structural basis of the significant decrease in the average lifetimes of PMal in CaM_{ox}, we have measured the accessibility of PMal in CaM_{ox} to the water-soluble quencher TEMPAMINE (4-amino-2,2,6,6-tetramethyl-1-piperidinyloxyl). As the extent of oxidative modification is increased, there is a small but progressive increase in the apparent Stern-Volmer quenching constant (K_{sv}) associated with PMal that correlates with the level of oxidative modification for both calcium-saturated and apo-CaM (Fig. 12). The greater solvent accessibility of PMal in CaM_{ox} is consistent with the large decrease in the average fluoresence lifetime of PMal (Table 3), and suggests that the oxidative modification of methionine to the corresponding methionine sulfoxide disrupts tertiary packing interactions that result in a more open tertiary structure around Cys^{26} in CaM_{ox}. Significantly, methionine oxidation does not interfere with the large changes in solvent accessibility of PMal upon calcium activation (Fig. 12). These latter results are consistent with previous observations regarding the calcium-dependent binding of CaM_{ox} to the plasma membrane Ca-ATPase (Yao et al., 1996), and suggest that the amino-terminal domains of native and oxidatively modified CaM undergo similar structural changes upon calcium activation.

TABLE 3 Lifetime parameters recovered from multiexponential fits to PMal-CaM in the absence (D) and presence (DA) of the fluorescence resonance energy transfer acceptor nitrotyrosine*

Ligand	Fraction of CaM Oxidized	Sample	α_1	τ_1 (ns)	α_2	τ_2 (ns)	α_3	τ_3 (ns)	α_4	τ_4 (ns)	$\bar{\tau}$ (ns)	$\chi_R^{2\#}$
+ Calcium	Native	D	0.79 (0.02)	3.8 (0.1)	0.14 (0.01)	18.6 (0.2)	0.076 (0.004)	106 (5)			13.5 (0.8)	1.6 (54)
		DA	0.76 (0.02)	2.3 (0.2)	0.17 (0.01)	11.3 (0.4)	0.066 (0.002)	74 (5)			8.6 (0.5)	1.1 (79)
	32 ± 7%	D	0.74 (0.02)	3.1 (0.1)	0.21 (0.01)	11.6 (0.2)	0.059 (0.002)	89 (4)			9.9 (0.6)	1.2 (56)
		DA	0.70 (0.02)	1.9 (0.1)	0.25 (0.01)	7.7 (0.2)	0.052 (0.001)	65 (3)			6.3 (0.3)	1.6 (69)
	46 ± 6%	D	0.46 (0.03)	2.1 (0.1)	0.42 (0.01)	6.6 (0.2)	0.092 (0.004)	19.6 (0.2)	0.019 (0.001)	134 (6)	8.2 (0.4)	0.46 (9.2)
		DA	0.61 (0.02)	1.5 (0.1)	0.34 (0.02)	6.1 (0.2)	0.039 (0.001)	22.9 (0.6)	0.012 (0.001)	111 (4)	4.8 (0.3)	1.7 (10.3)
	58 ± 4%	D	0.56 (0.02)	1.7 (0.1)	0.40 (0.02)	7.0 (0.2)	0.033 (0.002)	33.6 (0.5)	0.008 (0.001)	185 (10)	6.4 (0.4)	0.6 (16)
		DA	0.56 (0.02)	0.9 (0.1)	0.40 (0.01)	4.5 (0.2)	0.035 (0.001)	24.9 (0.3)	0.006 (0.001)	139 (7)	4.3 (0.3)	1.6 (18)
	100%	D	0.61 (0.02)	1.3 (0.1)	0.32 (0.01)	4.9 (0.1)	0.052 (0.002)	24.2 (0.7)	0.012 (0.001)	132 (6)	5.2 (0.3)	1.3 (34)
		DA	0.61 (0.02)	0.6 (0.1)	0.32 (0.01)	3.0 (0.2)	0.050 (0.001)	14.3 (0.2)	0.011 (0.001)	89 (10)	2.6 (0.1)	1.4 (42)
+ EGTA	Native	D	0.61 (0.01)	3.4 (0.1)	0.25 (0.01)	14.8 (0.1)	0.138 (0.006)	97 (4)			19.2 (1.1)	1.1 (9.7)
		DA	0.64 (0.02)	2.7 (0.2)	0.24 (0.01)	13.4 (0.3)	0.121 (0.003)	82 (3)			14.9 (0.3)	1.1 (12)
	32 ± 7%	D	0.68 (0.02)	3.0 (0.1)	0.24 (0.01)	13.8 (0.2)	0.078 (0.002)	98 (3)			12.9 (0.7)	1.0 (13)
		DA	0.68 (0.01)	2.4 (0.1)	0.27 (0.01)	12.3 (0.2)	0.050 (0.001)	94 (3)			9.7 (0.6)	0.6 (5)
	46 ± 6%	D	0.58 (0.03)	2.0 (0.1)	0.36 (0.01)	10.2 (0.3)	0.041 (0.002)	59 (2)	0.023 (0.001)	80 (3)	9.0 (0.5)	0.7 (2.5)
		DA	0.54 (0.02)	1.7 (0.1)	0.39 (0.01)	6.4 (0.2)	0.059 (0.002)	26 (1)	0.014 (0.001)	108 (5)	6.4 (0.4)	0.8 (3.2)
	58 ± 4%	D	0.54 (0.02)	0.3 (0.1)	0.31 (0.01)	3.8 (0.1)	0.105 (0.005)	25 (1)	0.041 (0.001)	103 (6)	8.2 (0.5)	1.1 (4.3)
		DA	0.66 (0.02)	1.4 (0.1)	0.29 (0.01)	6.5 (0.1)	0.035 (0.001)	34 (1)	0.015 (0.001)	117 (6)	5.7 (0.3)	0.7 (3.6)
	100%	D	0.56 (0.02)	1.5 (0.1)	0.35 (0.01)	6.5 (0.2)	0.072 (0.003)	29 (1)	0.02 (0.001)	101 (5)	7.5 (0.4)	0.8 (4.8)
		DA	0.84 (0.02)	0.8 (0.1)	0.13 (0.01)	5.9 (0.2)	0.021 (0.001)	27 (1)	0.009 (0.001)	103 (7)	3.0 (0.2)	0.9 (5.2)

*Average amplitudes (α_i) and lifetimes (τ_i), obtained from three- or four-exponential fits to frequency domain data collected for donor (D) only (PM-CaM) and donor-acceptor (DA or PM-nitrotyrosine-CaM) native, 1-h, 2-h, 4-h, and 10-h oxidized calmodulin, are shown in Table 1. The error associated with the average lifetime is propagated using the following equations: $x = au + bv$, $\sigma_x^2 = a^2\sigma_u^2 + b^2\sigma_v^2$; $x = auv$, $\sigma_x^2/x^2 = a^2/u^2 + b^2/v^2$ (Bevington, 1969). #The χ_R^2 for a two- or three-exponential fit to the data is shown in brackets for comparison purposes. Experimental conditions: The medium buffer contained 0.25 M HEPES, 0.1 M KCl, 1 mM $MgCl_2$, and either 0.1 mM $CaCl_2$ ($+Ca^{2+}$) or 0.1 mM EGTA ($-Ca^{2+}$), pH 7.5. The temperature was 25°C. Calmodulin concentrations were 1.2 μM.

Spatial separation between opposing globular domains in CaM subsequent to the oxidative modification of methionine

To assess whether large-scale alterations in the average spatial arrangement between the opposing globular domains in CaM_{ox} occur as a result of oxidation, we have used fluorescence resonance energy transfer (FRET) to measure the average spatial separation between the donor PMal and nitrotyrosine[138] (which functions as a FRET acceptor; Fig. 1) in CaM_{ox}. These measurements and the resulting data were fit in the same way as described previously for PMal-CaM in the absence of nitrotyrosine[138] (Fig. 9). Independent of the extent of oxidative modification, we observe that the frequency domain data for each donor-acceptor pair involving either calcium-saturated (Fig. 8 *C*) or apo- (Fig. 8 *D*) CaM are shifted to a similar extent toward higher frequencies in comparison to that observed for donor only (Fig. 8, *A* and *B*), consistent with previous measurements indicating that nonradiative energy transfer occurs from PMal to nitrotyrosine in CaM (Yao et al., 1994; Yao and Squier, 1996). The amount of FRET calculated from the individual intensity decays obtained from each sample of native or oxidatively modified CaM (Table 3) permits the calculation of the apparent spatial separation (r_{app}) between PMal and nitrotyrosine[138] (Fig. 13), and these results suggest that the calcium-dependent structural coupling between the opposing globular domains is diminished upon CaM oxidation (Fig. 13). These FRET measurements indicate that whereas oxidative modification of methionines does not alter the local calcium-dependent structural changes in the vicinity of PMal (Fig. 8 and Table 3), methionine oxidation interferes with specific noncovalent interactions that modify the long-range structural coupling between the opposing globular domains of CaM_{ox}.

Similar average distances between PMal and nitrotyrosine[138] are obtained by using the lifetime parameters obtained from simultaneously fitting the frequency response associated with the three oxidatively modified CaM samples shown in Fig. 8 to a two-state model involving two different average structures of CaM (Table 4), which correspond to 19 ± 5 Å and 20 ± 3 Å for apo- and calcium-saturated CaM_{ox}, respectively. The large spatial separation between PMal and nitrotyrosine[138] in native and oxidatively modified CaM suggests that the structural coupling between the oxidative modification of methionines in the carboxyl-terminal globular domain and structural alterations near PMal probably do not involve direct contact interactions between the opposing globular domains. These latter results are furthermore consistent with the small (i.e., ~4 Å) decrease in r_{app} in CaM_{ox} relative to native CaM that is obtained if one approximates fully oxidized CaM as a homogeneous species (Fig. 13).

In the calculation of the apparent spatial separation (r_{app}) between the opposing globular domains of native and oxi-

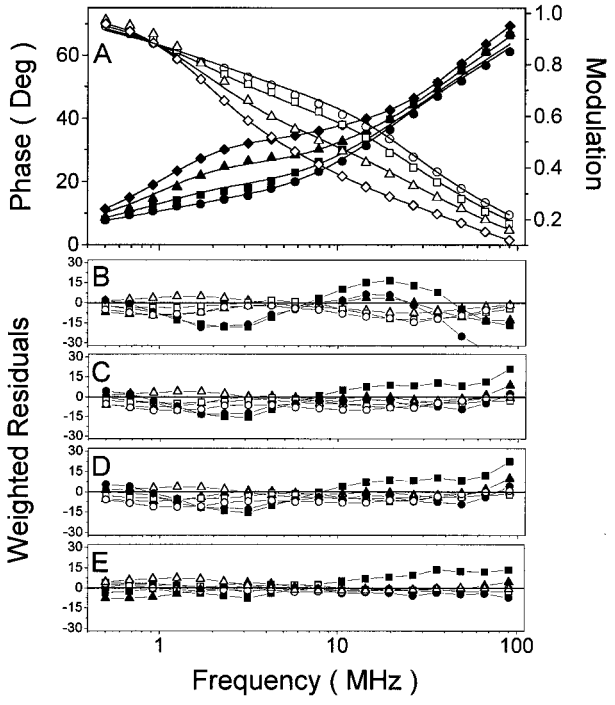

FIGURE 10 Simultaneous fitting of oxidatively modified CaM to a two-state model. Phase shift (◆, ▲, ■, ●) and modulation (◇, △, □, ○) data obtained for native PMal-CaM (◇, ◆) and subsequent to the exposure of CaM to H_2O_2 for 1, 2, and 4 h, which results in the respective oxidative modification of a methionine on 32 ± 7% (△, ▲), 46 ± 6% (□, ■), and 58 ± 4% (○, ●) of the CaM species. Conditions associated with the oxidative modification of CaM are fully described in Materials and Methods. The frequency domain data and the calculated best fit to a two-state model (N ⟷ O) are shown in *A*. The fitting procedure assumes that each CaM sample is a linear combination of these two states (see Eqs. 4 and 5 in Materials and Methods). In this model, N refers to the native structure of CaM, and O refers to the population of oxidatively modified CaM species whose structure is modified around PMal located at Cys^{26} in the amino-terminal domain. In the analysis of the data, the excited state properties of PMal for native CaM were fixed, and the average fluorescence properties (i.e., α_i's and τ_i's) and the amount of CaM (f_{ox}) whose structure is perturbed by methionine oxidation were recovered in the analysis of the data. The data were fit, assuming that the structurally perturbed population of oxidatively modified CaM could be fit to a multiexponential model. The weighted residuals (i.e., the difference between the experimental data and the calculated fit divided by the experimental uncertainty) are shown for a one-exponential (*B*), a two-exponential (*C*), a three-exponential (*D*), and a four-exponential fit to the data. The respective χ^2_R are 127, 61, 48, and 13. Lifetime measurements were made in buffer A in the presence of 0.1 mM $CaCl_2$ at 25°C (*A*).

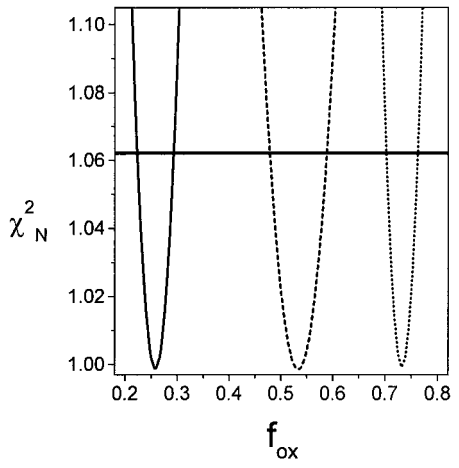

FIGURE 11 Normalized error surfaces for f_{ox} recovered for oxidatively modified CaM. Representative set of normalized chi-squared (χ^2_N) error surfaces obtained for the calculated fraction (f_{ox}) of CaM whose structure around PMal at Cys^{26} is altered upon methionine oxidation subsequent to exposure to H_2O_2 for 1 h (*solid line*), 2 h (*dashed line*), and 4 h (*dotted line*), is depicted for the frequency domain data set shown in Fig. 10 and is obtained by fixing the individual values of f_{ox} associated with a particular data set, and then minimizing the simultaneous fit associated with all four data sets to a two-state model (N ⟷ O), where $\chi^2_N = \chi^2_R/\chi^2_{R(minimum)}$. This analysis quantitatively accounts for the cross-correlation between the calculated f_{ox} and the recovered lifetime parameters (i.e., α_i's and τ_i's), as described previously (Beechem et al., 1991). The thick horizontal line at $\chi^2_N = 1.062$ corresponds to the *F*-statistic, which represents one-standard deviation relative to the best fit to the data. For comparison purposes, the actual distribution of oxidatively modified CaM species is documented in Table 2.

datively modified CaM, we have assumed that 1) the orientation between donor and acceptor chromophores is motionally averaged (i.e., $\kappa^2 = 2/3$), and 2) CaM_{ox} can be approximated as a single population. Whereas the major uncertainty in the calculation of molecular distances between sites on homogeneous samples from FRET data results from restrictions in the rotational dynamics of donor and acceptor chromophores whose relative orientation with respect to one another can modify the transfer efficiency (Dale and Eisinger, 1976; Haas et al., 1978; Dale et al., 1979; reviewed by Cheung, 1991), the small steady-state polarization ($P < 0.1$) of PMal indicates that the errors associated with the calculation of the distance between these sites are no larger than ~2 Å CaM, as previously discussed in detail for native CaM (Yao et al., 1994). It is therefore apparent that major uncertainty relating to the interpretation of the calculated distances between PMal and nitrotyrosine[138] result from the distribution of oxidatively modified CaM species present in these samples, and the apparent distance (r_{app}) represents a weighted average. However, irrespective of the model used to analyze the data, it is apparent that subsequent to exposure of CaM to H_2O_2 for 10 h (where essentially all CaM species contain at least one oxidatively modified methionine), there are no significant alterations in the spatial separation between the opposing globular domains upon calcium activation.

Rotational dynamics associated with PMal-CaM_{ox}

Time-resolved measurements of the rotational dynamics of chromophores at defined sites can provide additional information relating to changes in both the local environment and overall hydrodynamic properties of a protein (reviewed by Steiner, 1991). Therefore, to better define the structural alterations in CaM_{ox} that result from methionine oxidation, we have measured the frequency response of the modulated anisotropy and differential phase of PMal covalently bound

TABLE 4 Lifetime data for PMal-CaM$_{ox}$ derived from a two-state model*

Sample	α_1	τ_1 (ns)	α_2	τ_2 (ns)	α_3	τ_3 (ns)	α_4	τ_4 (ns)	$\bar{\tau}^{\#}$ (ns)	$\chi_R^{2\S}$	f_{oxi}¶ (1h)	f_{oxi}¶ (2h)	f_{oxi}¶ (4h)
+ Calcium PMal-CaM$_{native}$	0.79 (0.02)	3.8 (0.1)	0.14 (0.01)	18.6 (0.2)	0.076 (0.004)	106 (5)	—	—	13.5 (0.8)	1.4 (54)	—	—	—
PMal-CaM$_{native}$ + nitrotyrosine	0.76 (0.02)	2.3 (0.2)	0.17 (0.01)	11.3 (0.4)	0.066 (0.002)	74 (5)	—	—	8.6 (0.5)	1.1 (79)	—	—	—
PMal-CaM$_{ox}$[e]	0.59 (0.06)	1.83 (0.3)	0.39 (0.05)	8.0 (0.1)	0.016 (0.005)	43 (42)	0.002 (0.002)	355 (66)	5.7 (2.1)	13 (38)	0.26 (0.04)	0.54 (0.06)	0.74 (0.03)
PMal-CaM$_{ox}$ + nitrotyrosine‖	0.66 (0.04)	1.4 (0.3)	0.32 (0.05)	6.1 (1.6)	0.02 (0.01)	34 (28)	0.002 (0.002)	254 (117)	3.9 (1.9)	8.4 (58)	0.24 (0.03)	0.59 (0.04)	0.73 (0.04)
+ EGTA PMal-CaM$_{native}$	0.61 (0.01)	3.4 (0.1)	0.25 (0.01)	14.8 (0.1)	0.138 (0.006)	97 (4)	—	—	19.2 (1.1)	1.1 (10)	—	—	—
PMal-CaM$_{native}$ + nitrotyrosine	0.64 (0.02)	2.7 (0.2)	0.24 (0.01)	13.4 (0.3)	0.121 (0.003)	82 (3)	—	—	14.9 (0.3)	1.1 (12)	—	—	—
PMal-CaM$_{ox}$[e]	0.64 (0.09)	1.9 (0.4)	0.30 (0.05)	9.4 (1.7)	0.05 (0.01)	55 (18)	0.002 (0.002)	203 (69)	7.4 (2.6)	15.9 (41)	0.32 (0.05)	0.76 (0.06)	0.87 (0.06)
PMal-CaM$_{ox}$ + nitrotyrosine[e]	0.62 (0.06)	0.9 (0.4)	0.32 (0.09)	4.8 (0.3)	0.06 (0.02)	26 (16)	0.003 (0.002)	136 (45)	4.0 (2.1)	23.7 (34)	0.23 (0.07)	0.54 (0.16)	0.77 (0.23)

*Average amplitudes (α_i) and lifetimes (τ_i), obtained from three- or four-exponential fits to frequency domain data collected for donor only (D or PMal-CaM) and donor-acceptor (DA or PMal-TNM-CaM) CaM. The uncertainties represent the maximal variance associated with a rigorous analysis of the correlated errors between the fitting parameters relative to the parameter of interest, as previously described (Beechem et al., 1991; Yao et al., 1994). The medium buffer contained 1.2 μM CaM in Buffer A and either 0.1 mM $CaCl_2$ or 0.1 mM EGTA at 25°C.

[#]The amplitude weighted average lifetime ($\bar{\tau}$) is calculated as: $\bar{\tau} = \Sigma\alpha_i\tau_i$, and is proportional to the quantum yield of PMal-CaM (Luedtke et al., 1981). The associated errors were propagated as described in Bevington (1969).

[§]The χ_R^2 for a simpler two- or three-exponential fit to the data is shown in brackets for comparison purposes.

¶f_{ox} (1 h), f_{ox} (2 h), and f_{ox} (4 h) represent the calculated fraction that contains a structurally altered (oxidatively modified) population of CaM around PMal at Cys[26], that is, associated with CaM samples that were exposed to H_2O_2 for 1 h, 2 h, and 4 h, as described by Eqs. 4 and 5 in Materials and Methods. The total average number of methionines oxidized in these samples was separately determined to be, respectively, 0.17 ± 0.07, 0.31 ± 0.16, 0.57 ± 0.09 (Yao et al., 1996).

‖The lifetime of CaM$_{ox}$ was recovered as described by Eqs. 4 and 5 in Materials and Methods.

to Cys[26] in native CaM in four different samples of CaM with variable levels of oxidative modification, corresponding to an average of 0.40 ± 0.03, 0.58 ± 0.05, 0.72 ± 0.06, and 1.5 ± 0.1 methionine sulfoxides per CaM (Table 2). Representative data of both calcium-saturated and apo-CaM are shown in Fig. 14 for native CaM and after exposure to H_2O_2 for 10 h, which results in the oxidative modification of methionines in essentially all CaM species (Table 2). In all cases the data can be adequately fit to a model assuming two rotational correlation times, as evidenced by 1) the greater than 10-fold improvement in the χ^2_R relative to a model involving a single rotational correlation time and 2) the nearly randomly weighted residuals (Fig. 14). Qualitatively, one observes that the frequency response is very similar irrespective of methionine oxidation, suggesting that there are no large alterations in the tertiary structure of CaM$_{ox}$ relative to native CaM. Previous measurements indicate that the longer of the two rotational correlation times (ϕ_2) for native calcium-saturated CaM (i.e., ϕ_2 = 10.9 ± 0.7 ns; Table 5) corresponds to the rotational motion along the principal axis of CaM (Small and Anderson, 1988; Yao et al., 1994) and is sensitive to changes in the overall molecular dimensions of CaM. The more rapid rotational correlation time (i.e., $\phi_1 \approx 1$ ns; Table 5) is associated with the independent segmental rotational dynamics of PMal, and is sensitive to alterations in the local environment around Cys[26]. Whereas the structural heterogeneity associated with the populations of oxidatively modified CaMs prevents a quantitative consideration of the measured rotational correlation times, alterations in the average rates of the segmental rotational dynamics of PMal and overall rotational dynamics of CaM$_{ox}$ provide important informa-

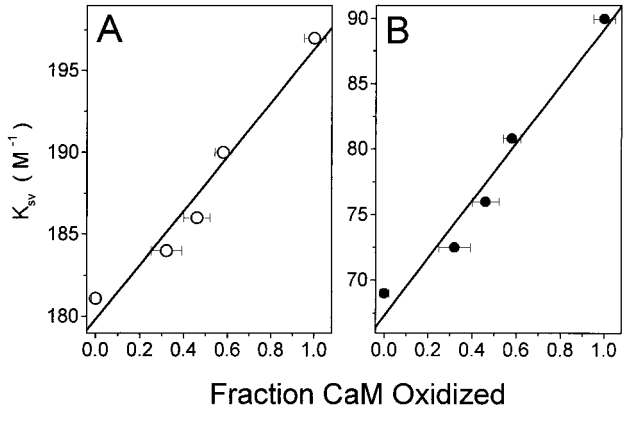

FIGURE 12 Enhanced solvent accessibility of PMal upon oxidative modification of methionine in CaM. The apparent Stern-Volmer (K_{sv}) quenching constants for PMal located at Cys[26] in calcium binding loop I to the water-soluble quencher TEMPAMINE were determined in the presence of either 0.1 mM $CaCl_2$ (*A*) or 0.1 mM EGTA (*B*) in buffer A for CaM samples containing variable levels of oxidative modification. The concentration of CaM was 1.2 μM. The sample temperature was 25°C. Lines represent the relationship between surface accessibility and the fraction of CaM that contains an oxidatively modified methionine obtained from a linear regression [$F(x) = mx + b$], in which the sum of the squared deviations between the experimental data and the fit is minimized. For calcium-saturated CaM, $m = 17 \pm 2\ M^{-1}\ s^{-1}$ and $b = 180 \pm 1\ M^{-1}$. For apo-CaM, $m = 22 \pm 2\ M^{-1}\ s^{-1}$ and $b = 67 \pm 1\ M^{-1}$.

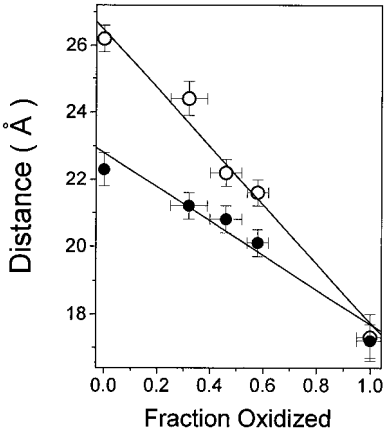

FIGURE 13 Methionine oxidative disrupts calcium-dependent changes in the spatial separation between the opposing globular domains of CaM. The apparent average spatial separation between PMal located at Cys^{26} and nitrotyrosine[138] for samples of apo- (●) and calcium- (○) saturated CaM that were exposed to H_2O_2 for various periods of time was calculated from the lifetime data in Table 3, using the following formula:

$$E = 1 - \frac{\bar{\tau}_{da} - \bar{\tau}_d \times (1 - f_a)}{\bar{\tau}_d \times f_a} = \frac{R_o^6}{R_o^6 + r^6}.$$

E is the corrected fluorescence resonance energy transfer efficiency, which takes into account the incomplete nitration of tyrosine (i.e., $f_a = 0.95 \pm 0.04$), $\bar{\tau}_d$ is the average lifetime of PMal-CaM, $\bar{\tau}_{da}$ is the average lifetime of PMal-CaM in the presence of nitrotyrosine[138], r is the apparent spatial separation between PMal and nitrotyrosine, and R_o is the Förster critical distance, where $E = 0.50$ (Fairclough and Cantor, 1978). For native CaM, $R_o = 20.6$ Å (Yao et al., 1994). Oxidative modification of methionines in CaM_{ox} does not alter the overlap integral (J) between PMal and nitrotyrosine. The apparent R_o (in cm) associated with each PMal-CaM_{ox} sample can therefore be estimated by correcting for alterations in the quantum yield (ϕ) upon oxidative modification, using the following relationships:

$$R_o = 9.79 \times 10^{-5} \times (\kappa^2 \times \eta^{-4} \times \phi_{PMal-CaM} \times J)^{1/6},$$

where

$$\phi_{PMal-CaM_{ox}} = \frac{\bar{\tau}_{PMal-CaM_{ox}}}{\bar{\tau}_{PMal-CaM_{native}}} \times \phi_{PMal-CaM_{native}}.$$

The calculation of R_o assumes rapid reorientation between PMal and nitrotyrosine[138] (i.e., $\kappa_2 = 0.667$) and the refractive index of water (i.e., $\eta = 1.4$). J was determined to be 2.8×10^{-15} M^{-1} cm^3 for both calcium-saturated native and oxidatively modified PMal-CaM. Lines represent the relationship between distance and the fraction of CaM that contains an oxidatively modified methionine obtained from a linear regression [$F(x) = mx + b$], in which the sum of the squared deviations between the experimental data and the fit is minimized. For calcium-saturated CaM, $m = -8.7 \pm 0.8$ Å and $b = 26.5 \pm 0.4$ Å. For apo-CaM, $m = -5.1 \pm 0.7$ Å and $b = 22.8 \pm 0.4$ Å.

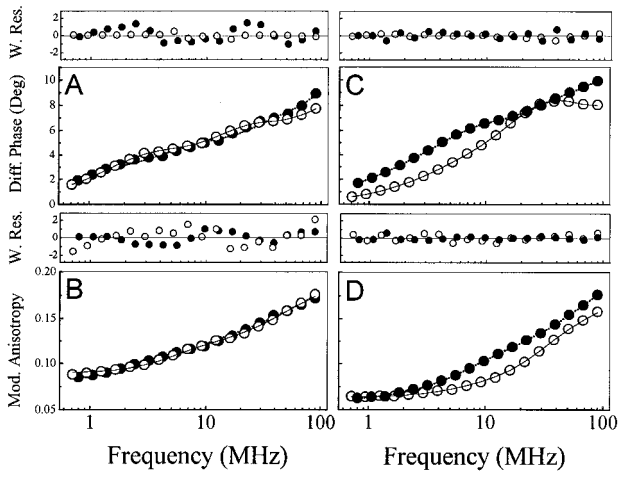

FIGURE 14 Frequency domain fluorescence anisotropy data for native and oxidatively modified CaM. Differential phase angle (*A*, *C*) and modulated anisotropy (*B*, *D*) of native CaM (○) or subsequent to exposure to H_2O_2 for 10 h (i.e., CaM_{ox}; ●) for calcium-saturated (*A*, *B*) and apo- (*C*, *D*) CaM. Lines represent the best fit to the data. Weighted residuals correspond to the experimental data minus the calculated value for the two-exponential experimental fit normalized by the assumed standard errors for the measurements, which were respectively assumed to be 0.2° and 0.005 for the differential phase and modulated anisotropy. Experimental conditions involved 1.2 μM PMal-CaM in buffer A in the presence of either 0.1 mM $CaCl_2$ (*A*, *B*) or 0.1 mM EGTA (*C*, *D*). The sample temperature was 25°C.

tion relating to possible alterations in the tertiary structure of CaM.

Upon the oxidative modification of methionine, there is a progressive decrease in the apparent rotational correlation times associated with both the segmental rotational motion (ϕ_1) of PMal and the overall rotational dynamics (ϕ_2) of CaM (Fig. 15). The enhanced segmental rotational dynamics ($1/\phi_1$) observed upon methionine oxidation is consistent with the larger solvent accessibility of PMal for these samples (Fig. 12), and suggests that methionine sulfoxide disrupts noncovalent interactions that function to stabilize the tertiary structure of native CaM. The faster overall rotational diffusion (i.e., $1/\phi_2$) of CaM_{ox} relative to native CaM suggests that there are global structural changes in CaM_{ox} that modify its hydrodynamic properties relative to native CaM. However, whereas there is an increase in the segmental rotational dynamics of PMal upon calcium binding in both native and oxidatively modified CaM (Fig. 15 *A*), the large calcium-dependent increase in the rotational correlation time associated with overall rotational motion observed in native CaM is greatly diminished in CaM_{ox} (Fig. 15 *B*). These results indicate that methionine oxidation does not primarily interfere with the calcium-dependent structural changes in the amino-terminal domain that result in the reorientation of α-helical structural elements with respect to one another, resulting in a more open tertiary structure (Yao et al., 1994; Zhang et al., 1995), but rather alters the calcium-dependent structural coupling between the opposing globular domains of CaM_{ox}. These results are consistent, furthermore, with the ESI-MS and quenching data (Figs. 2, 5, and 12), which respectively indicate that methionine oxidation results in relatively small structural changes involving the amino- and carboxyl-terminal domains, and like the FRET measurements (Fig. 13), suggest that oxidation may instead alter the structural coupling between the opposing domains through alterations in the conformational features involving the interdomain central helix.

TABLE 5 Rotational dynamics of PM-CaM$_{ox}$*

Fraction CaM oxidized	Ligand	$P^{\#}$	g_1r_o[§]	ϕ_1 (ns)[§]	g_2r_o[§]	ϕ_2 (ns)[§]	$\chi_R^{2\P}$
Native	+ Calcium	0.078	0.16 (0.01)	0.8 (0.1)	0.11 (0.01)	10.9 (0.7)	0.80 (15.6)
	+ EGTA	0.059	0.13 (0.01)	1.4 (0.1)	0.11 (0.01)	8.8 (0.5)	0.62 (18.7)
32 ± 7%	+ Calcium	0.078	0.14 (0.01)	0.8 (0.1)	0.13 (0.01)	10.6 (0.4)	0.56 (21.2)
	+ EGTA	0.059	0.17 (0.01)	1.2 (0.1)	0.10 (0.01)	9.0 (0.7)	0.94 (29.8)
46 ± 6%	+ Calcium	0.078	0.17 (0.01)	0.7 (0.1)	0.12 (0.01)	11.0 (0.3)	0.58 (13.7)
	+ EGTA	0.059	0.19 (0.01)	1.0 (0.1)	0.10 (0.01)	8.7 (0.6)	0.86 (24.6)
58 ± 4%	+ Calcium	0.078	0.14 (0.01)	0.6 (0.1)	0.17 (0.01)	10.0 (0.2)	0.67 (19.7)
	+ EGTA	0.059	0.14 (0.01)	1.0 (0.1)	0.16 (0.01)	8.4 (0.2)	0.72 (18.9)
100%	+ Calcium	0.078	0.18 (0.01)	0.5 (0.1)	0.12 (0.01)	8.8 (0.2)	0.76 (29.5)
	+ EGTA	0.058	0.18 (0.01)	0.9 (0.1)	0.12 (0.01)	8.4 (0.2)	0.72 (21.8)

*Reported rotational correlation times (ϕ_i) and their associated amplitudes ($g_i \times r_o$) were obtained for a multiexponential fit to the differential phase and modulated anisotropy data, as described in Materials and Methods.

[#]P is the measured steady-state polarization.

[§]g_ir_o are the amplitudes of the total anisotropy decay associated with each rotational correlation time (ϕ_i), where ϕ_1 and ϕ_2 are the average rotational correlation times associated with the segmental and overall rotational motion of the distribution of native and oxidatively modified CaM species.

[¶]χ^2_R describes the deviations between the model and experimental data, and the number in parentheses represents the χ^2_R obtained from a one-component fit to the data. Experimental conditions are described in the legend of Fig. 14. Frequency-independent experimental errors of 0.2° and 0.005, respectively, were assumed in fitting the differential phase and modulated anisotropy.

DISCUSSION

Summary of results

Using ESI-MS, we have identified two isoforms of CaM expressed in wheat germ. The oxidative modification of a single methionine in either sequence results in no large-scale alteration of the secondary or tertiary structures of either globular domain, because there is little or no change in 1) the solvent accessibility of additional methionines to oxidative modification by H_2O_2 (Figs. 2 and 5), 2) the CD spectrum (Fig. 6 *A*), 3) the solvent exposure or segmental rotational dynamics of PMal located at Cys[26] in the amino-terminal domain (Figs. 12 and 15 *A*), 4) the spatial separation between PMal and nitrotyrosine[138] located in the opposing globular domains (Fig. 13), or 5) the overall rotational correlation time (Fig. 15 *B*). However, oxidative modification of methionines located in the carboxyl-terminal domain does result in a large decrease in the average lifetime of PMal in the amino-terminal domain (Figs. 8–10), indicating that there are concerted structural changes involving the amino-terminal domain upon oxidative modification of methionines located in the carboxyl-terminal domain. Furthermore, whereas the calcium-dependent structural changes associated with the amino-terminal domain are preserved upon oxidative modification (Figs. 8, 12, and 15 A), the global structural coupling between the opposing globular domains that are normally associated with calcium activation is diminished upon methionine oxidation (Figs. 13 and 15 *B*). Because there is a large spatial separation between the opposing globular domains in both apo- and calcium-saturated CaM for both native and oxidatively modified CaM (Fig. 13), these results suggest that the loss of conformational coupling between the opposing globular domains in oxidatively modified CaM involves structural alterations involving the interdomain central helix.

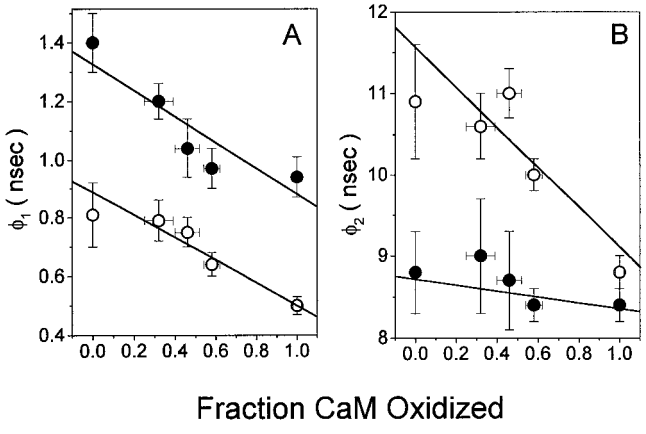

FIGURE 15 Increased rotational dynamics of PMal in oxidatively modified CaM. Average values of the segmental (*A*) and global (*B*) rotational dynamics of PMal for calcium saturated (○) and apo-CaM (●) were measured for PMal-CaM that contained variable amounts of methionine oxidation, as tabulated in Table 2. Experimental conditions are as described in the legend to Fig. 14. Error bars represent the maximum variance associated with the best fit to the data obtained from the χ^2_N error surfaces, and are tabulated in Table 5. Lines represent the relationship between rotational correlation times and the fraction of CaM that contains an oxidatively modified methionine obtained from a linear regression [$F(x) = mx + b$], in which the sum of the squared deviations between the experimental data and the fit is minimized. In *A*, $m = -0.39 \pm 0.05$ ns and $b = 0.88 \pm 0.04$ ns for calcium-saturated CaM, whereas $m = -0.44 \pm 0.12$ ns and $b = 1.32 \pm 0.07$ ns for apo-CaM. In *B*, $m = -2.9 \pm 0.6$ ns and $b = 11.8 \pm 0.4$ ns for calcium-saturated CaM, whereas $m = -0.4 \pm 0.2$ ns and $b = 8.7 \pm 0.2$ ns for apo-CaM.

Relationship to other studies

A large body of evidence including kinetics of chemical modification, binding of hydrophobic reagents, dynamics of segmental and global rotational motions, and proteolytic susceptibility of CaM indicates that structural transitions associated with calcium binding in each of the opposing globular domains of CaM are conformationally coupled to structural transitions in the other domain (Klee, 1977;

Seamon, 1980; Johnson, 1983; Yoshida et al., 1983; Thulin et al., 1984; Wang et al., 1984; Babu et al., 1988; MacKall and Klee, 1991; Maune et al., 1992; Török et al., 1992; Kilhouffer et al., 1992; Yao et al., 1994; Pedigo and Shea, 1995a,b; Mukherjea et al., 1996; Sorensen and Shea, 1996). Likewise, the construction of mutant CaMs with altered calcium affinity in calcium-binding sites III or IV in the carboxyl-terminal domain of CaM alters the calcium-dependent conformational coupling between the opposing globular domains (Starovasnik et al., 1992; Shea et al., 1996). In agreement with these results, we find that the lifetime of PMal bound to Cys^{26} in the amino-terminal domain is sensitive to oxidative modification of methionines in the carboxyl-terminus (see above). Possible clues regarding the structural basis for the loss of the calcium-dependent conformational coupling between the opposing globular domains upon methionine oxidation are apparent upon consideration of the long-range noncovalent interactions present in the crystal structure of CaM (Fig. 16 *A*), because the hydrogen bond between Tyr^{138} and Glu^{82} has been suggested to stabilize the interdomain central helix (Babu et al., 1988; Chattopadhyaya et al., 1992; Mukherjea et al., 1996). Furthermore, two methionines at the carboxyl-terminus (i.e., Met^{145} and Met^{146}) are proximal to Tyr^{138}, represent the primary sites of oxidative modification, and have been suggested to play a critical role in binding target proteins (Meador et al., 1992, 1993; reviewed by Crivici and Ikura, 1995). It is therefore possible that the oxidation of one of these carboxyl-terminus methionines may modify specific noncovalent interactions such as those between Tyr^{138} and Glu^{82} that normally function to stabilize the structure of the central helix. Furthermore, because the interdomain central helix is known to be only marginally stable in solution (Barbato et al., 1992), the loss of a limited number of stabilizing interactions might be expected to result in alterations in the structure of the central helix.

Furthermore, the proposed functional linkage between the oxidative modification of a carboxyl-terminus methionine, the disruption of the hydrogen bond between Tyr^{138} and Glu^{82}, and the inability of CaM_{ox} to activate the PM-Ca-ATPase are consistent with other measurements involving 1) the substitution of phenylalanine for the equivalent tyrosine in vertebrate CaM (i.e., Tyr^{138}), which has a reduced ability to activate the PM-Ca-ATPase (Sacks et al., 1996); 2) the substitution or deletion of Glu^{82} in vertebrate CaM, which results in structural alterations with respect to the overall dimensions of CaM and in the diminished ability of CaM to activate some target proteins (Craig et al., 1987; Kataoka et al., 1991); and 3) the substitution of either Arg or Val for Met^{145} in vertebrate and paramecium CaM

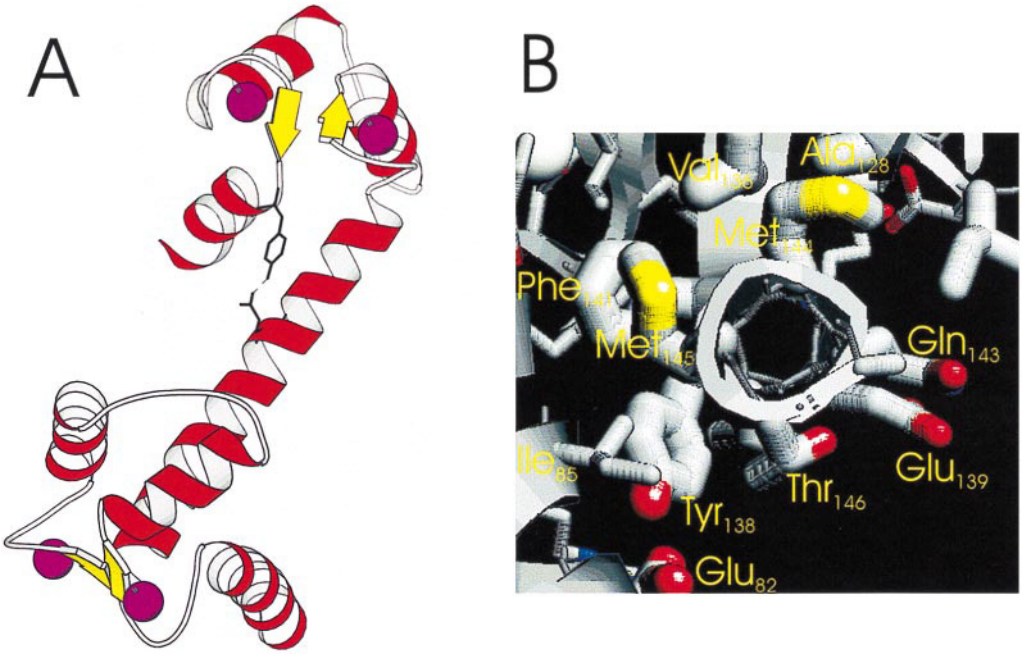

FIGURE 16 Representation of long-range stabilizing interactions apparent in the crystal structure of calcium-activated CaM. (*A*) Ribbon diagram depicting long-range hydrogen bond between Tyr^{138} and Glu^{82} observed in the crystal structure of calcium-saturated vertebrate CaM (Babu et al., 1988; Chattopadhyaya et al., 1992), which has been suggested to stabilize the interdomain central helix (Babu et al., 1988; Mukherjea et al., 1996). Secondary structural elements representing the α-helical backbone (*red*) and antiparallel β-sheet structure (*yellow*) are indicated, and side chains associated with Tyr^{138} and Glu^{82} are illustrated by a stick representation. The four calcium ligands are drawn using their van der Waals radii (*purple*). (*B*) A depiction of the orientation of amphipathic α-helix located at the carboxyl-terminus of CaM within the tertiary structure of calcium-saturated vertebrate CaM emphasizes the possible relationship between the orientation and secondary structure around Tyr^{138} and noncovalent interactions that stabilize the native tertiary structure. Amino acid side chains are drawn as tubes, and individual elements correspond to carbon (*white*), oxygen (*red*), sulfur (*yellow*), and nitrogen (*blue*). The protein backbone is connected by a ribbon to better differentiate protein secondary structural elements. Illustrations in *A* and *B* were drawn using atomic coordinates 1cll.pdb, with, respectively, the programs MOLSCRIPT and RASMOL (Kraulis, 1991; Sayle and Milner, 1995).

(equivalent to Met^{146} in wheat germ CaM), which respectively result in an inability to activate either purified phosphodiesterase or the calcium-dependent potassium currents in paramecium (Zhang et al., 1994; Kung et al., 1992). However, whereas the formation of methionine sulfoxide in CaM_{ox} results in long-range structural perturbations involving both globular domains, the substitution of Gln for either Met^{144} or Met^{145} in vertebrate CaM does not perturb the tertiary structures of CaM or significantly alter its ability to activate a range of different target proteins, including the PM-Ca-ATPase (Chin and Means, 1996; Yin and Squier, unpublished observations). Likewise, the substitution of Leu for either of these carboxyl-terminal methionines does not significantly affect the ability of CaM to activate phosphodiesterase (Zhang et al., 1994), suggesting that subtle changes in the size and polarity of the amino acid side chains at these positions have little structural or functional effect with respect to the ability of CaM to activate target proteins. Therefore, the polarity changes associated with methionine sulfoxide formation do not explain why CaM_{ox} functions as an inhibitor with respect to the activation of the PM-Ca-ATPase by native CaM. These results suggest that the functional effects associated with methionine sulfoxide formation in CaM are not the result of alterations in specific binding interactions between PM-Ca-ATPase and individual methionine residues in CaM.

A consideration of the crystal structure of the carboxyl-terminal amphipathic α-helix (located between Tyr^{138} and Ala^{147}) in vertebrate CaM offers further insight regarding the reasons why the substitution of valine, arginine, or methionine sulfoxide for one of the carboxyl-terminal methionines may alter the ability of CaM to activate some target enzymes, whereas Gln or Leu have little functional affect. Met^{144} and Met^{145} in vertebrate CaM are located on the hydrophobic face of the helix (Fig. 16 *B*) and participate in van der Waals contact interactions with nonpolar side chains involving both the central helix (i.e., Ile^{85}) and other amino acids in the carboxyl terminus (i.e., Ala^{128}, Val^{136}, and Phe^{141}) that act to stabilize the orientation of this helix. The substitution of a charged amino acid such as Arg on the hydrophobic face of this α-helix would be expected to reorient the α-helical backbone toward polar water. This could result in the disruption of long-range noncovalent bonds, such as the hydrogen bond between Tyr^{138} and Glu^{82}, that may normally function to stabilize the backbone conformation of CaM. On the other hand, Val, like methionine sulfoxide, contains a bulky hydrophobic side chain that does not pack well in an α-helix (Richardson and Richardson, 1989), and may disrupt aspects of the secondary structure and other noncovalent interactions involving the carboxyl-terminus that likewise disrupt long-range noncovalent interactions. The suggestion that methionine sulfoxide formation alters the structure of the carboxyl-terminus α-helix is furthermore consistent with the ability of methionine sulfoxide to block the formation of higher structural elements involving the formation of coiled-coils in model peptides (Garcia-Echeverria, 1996), indicating that methionine sulfoxide can induce large-scale structural changes in proteins. In contrast, Gln and Leu pack efficiently into an α-helix, and are not expected to alter the structure of the carboxyl-terminal α-helix or specific noncovalent interactions associated with the native structure of CaM (Richardson and Richardson, 1989).

CONCLUSIONS AND FUTURE DIRECTIONS

Oxidative modification of a limited number of methionines in CaM results in long-range structural changes that function to decrease the stability of CaM, and disrupts the concerted calcium-dependent structural changes involving the conformational coupling between the opposing globular domains in CaM that are normally involved in calcium activation. These results may explain, in part, the functional sensitivity of CaM to oxidative modification. Future measurements should investigate the potential role of specific noncovalent interactions, such as those involving the hydrogen bond between Tyr^{138} and Glu^{82}, with respect to the structure and stability of the interdomain central helix and the spatial arrangement of the opposing globular domains in CaM.

We wish to thank Sam George for providing a cDNA encoding vertebrate CaM, Diana J. Bigelow for insightful discussions, Ms. Homigol Biesiada of the KU Mass Spectrometry Laboratory for her efforts in acquiring the FAB and ESI spectra, and Ms. Nancy Harmony for her help in preparing the manuscript.

Supported by the National Institutes of Health (grants AG12993 and GM46837) and the American Heart Association (grant 1697). The tandem mass spectrometer and electrospray source were respectively obtained through grants from the National Institutes of Health (S10 RR0 6294) and the National Science Foundation (CHE-9413975). ZQ is supported by a fellowship from the American Heart Association.

REFERENCES

Alber, T. 1989. Stabilization energies of protein conformation. *In* Prediction of Protein Structure and the Principles of Protein Conformation. G. D. Fasman, editor. Plenum Press, New York. 161–192.

Alexianu, M. E., B.-K. Ho, A. H. Mohamed, V. La Bella, R. G. Smith, and S. H. Appel. 1994. The role of calcium-binding proteins in selective motor neuron vulnerability in amyotrophic lateral sclerosis. *Ann. Neurol.* 36:846–858.

Babu, Y. S., C. E. Bugg, and W. J. Cook. 1988. Structure of calmodulin refined at 2.2 Å resolution. *J. Mol. Biol* 204:191–204.

Barbato, G., M. Ikura, L. Kay, R. W. Pastor, and A. Bax. 1992. Backbone dynamics of calmodulin studied by ^{15}N relaxation using inverse detected two-dimensional NMR spectroscopy: the central helix is flexible. *Biochemistry.* 31:5269–5278.

Bayley, P. M., and S. R. Martin. 1992. The α-helical content of calmodulin is increased in solution conditions favouring protein crystallization. *Biochim. Biophys. Acta.* 1160:16–21.

Becktel, W. J., and J. A. Schellman. 1987. Protein stability curves. *Biopolymers.* 26:1859–1877.

Beechem, J. M., E. Gratton, M. Ameloot, J. R. Knutson, and L. Brand. 1991. The global analysis of fluorescence intensity and anisotropy decay data: second generation theory and programs. *In* Topics in Fluorescence Spectroscopy, Vol. 2. J. R. Lakowicz, editor. Plenum Press, New York. 1–52.

Bevington, P. R. 1969. Data Reduction and Error Analysis for the Physical Sciences. McGraw-Hill, New York.

Breton, C., A. Chaboud, E. Matthys-Rochon, E. E. M. Bates, J. M. Cock, H. Fromm, and C. Dumas. 1995. PCR-generated cDNA library of transition-stage maize embryos: cloning and expression of calmodulin genes during early embryogenesis. *Plant Mol. Biol.* 27:105–113.

Carafoli, E. 1987. Intracellular calcium homeostasis. *Annu. Rev. Biochem.* 56:395–433.

Chattopadhyaya, R., W. E. Meador, A. R. Means, and F. A. Quiocho. 1992. Calmodulin structure refined at 1.7 Å resolution. *J. Mol. Biol.* 228: 1177–1192.

Chen, Y.-L., B. A. Collings, and D. J. Douglas. 1997. Collision cross sections of myoglobin and cytochrome c ions with Ne, Ar, and Kr. *J. Am. Soc. Mass Spectrom.* 8:681–687.

Cheung, H. C. 1991. Resonance energy transfer. *In* Topics in Fluorescence Spectroscopy, Vol. 2. J. R. Lakowicz, editor. Plenum Press, New York. 128–176.

Chin, D., and A. R. Means. 1996. Methionine to glutamine substitutions in the C-terminal domain of calmodulin impair the activation of three protein kinases. *J. Biol. Chem.* 29:30465–30471.

Chye, M. L., C. M. Liu, and C. T. Tan. 1995. A cDNA clone encoding *Brassica* calmodulin. *Plant Mol. Biol.* 27:419–423.

Coyle, J. T., and P. Puttfarcken. 1993. Oxidative stress, glutamate, and neurodegenerative disorders. *Science.* 262:689–695.

Craig, T. A., D. M. Watterson, F. G. Prendergast, J. Haiech, and D. M. Roberts. 1987. Site-specific mutagenesis of the alpha-helices of calmodulin. Effect of altering a charge cluster in the helix that links the two halves of calmodulin. *J. Biol. Chem.* 262:3278–3284.

Crivici, A., and M. Ikura. 1995. Molecular and structural basis of target recognition by calmodulin. *Annu. Rev. Biophys. Biomol. Struct.* 24: 85–116.

Dale, R. E., and J. Eisenger. 1976. Intramolecular energy transfer and molecular conformation. *Proc. Natl. Acad. Sci. USA.* 73:271–273.

Dale, R. E., J. Eisenger, and W. E. Blumberg. 1979. The orientational freedom of molecular probes. The orientation factor in intramolecular energy transfer. *Biophys. J.* 26:161–193.

Ehrhardt, M. R., L. Erijman, G. Weber, and A. J. Wand. 1996. Molecular recognition by calmodulin: pressure-induced reorganization of a novel calmodulin-peptide complex. *Biochemistry.* 35:1599–1605.

Fairclough, R. H., and C. R. Cantor. 1978. The use of singlet-singlet energy transfer to study macromolecular assemblies. *Methods Enzymol.* 48: 347–379.

Finn, B. E., J. Evenäs, D. Drakenberg, J. P. Waltho, E. Thulin, and S. Forsén. 1995. Calcium-induced structural changes and domain autonomy in calmodulin. *Nature Struct. Biol.* 2:777–783.

Fliss, H., and G. Docherty. 1987. Oxidation of methionine in proteins of isolated rat heart myocytes and tissue slices by neutrophil-generated oxygen radicals. *Dev. Cardiovasc. Med.* 67:85–98.

Galaud, J. P., J. J. Lareyre, and N. Boyer. 1993. Isolation, sequencing and analysis of the expression of Bryonia calmodulin after mechanical perturbation. *Plant Mol. Biol.* 23:839–846.

Garcia-Echeverria, C. 1996. Disruption of coiled coil formation by methionine oxidation. *Bioorg. Med. Chem. Lett.* 6:229–232.

Grand, R. J. A., and S. V. Perry. 1978. Amino acid sequence of the troponin C-like protein (modulator protein) from bovine uterus. *FEBS Lett.* 92:137–142.

Griess, E. A., G. L. Igloi, and G. Feix. 1994. Isolation and sequence comparison of a maize calmodulin cDNA. *Plant Physiol.* 104: 1467–1468.

Haas, E., E. Katchalski-Katzir, and I. Steinberg. 1978. Effect of the orientation of donor and acceptor on the probability of energy transfer involving electronic transitions of mixed polarization. *Biochemistry.* 17:5064–5070.

Harman, D. 1987. The free-radical theory of aging. *In* Modern Biological Theories of Aging. R. N. Butler, E. L. Schneider, R. L. Sprott, and H. R. Warner, editors. Raven Press, New York. 81–87.

Heidorn, D. B., and J. Trewhella. 1988. Comparison of the crystal and solution structures of calmodulin and troponin C. *Biochemistry.* 27: 909–915.

Hühmer, A. F. R., N. C. Gerber, P. R. Ortiz de Montellano, and Ch. Schöneich. 1996. Peroxynitrite reduction of calmodulin stimulation of neuronal nitric oxide synthase. *Chem. Res. Toxicol.* 9:484–491.

James, P., T. Vorherr, and E. Carafoli. 1995. Calmodulin-binding domains: just two faced or multi-faceted? *Trends Biochem. Sci.* 20:38–42.

Jena, P. K., A. S. N. Reddy, and B. W. Poovaiah. 1989. Molecular cloning and sequencing of a cDNA for plant calmodulin: signal-induced changes in the expression of calmodulin. *Proc. Natl. Acad. Sci. USA.* 86: 3644–3648.

Johnson, J. D. 1983. Allosteric interactions among drug binding sites on calmodulin. *Biochem. Biophys. Res. Commun.* 112:787–793.

Johnson, M. L., and L. M. Faunt. 1992. Parameter estimation by least-squares methods. *Methods Enzymol.* 210:1–37.

Kataoka, M., J. F. Head, A. Persechini, R. H. Kretsinger, and D. M. Engelman. 1991. Small angle x-ray scattering studies of calmodulin mutants with deletions in the linker region of the central helix indicate that the linker region retains a predominantly alpha-helical conformation. *Biochemistry.* 30:1188–1192.

Khachaturian, Z. S. 1994. Calcium hypothesis of Alzheimer's disease and brain aging. *Ann. N.Y. Acad. Sci.* 747:1–11.

Kilhouffer, M. C., M. Kubina, F. Travers, and J. Haiech. 1992. Use of engineered proteins with internal tryptophan reporter groups and perturbation techniques to probe the mechanism of ligand-protein interactions: investigation of the mechanism of calcium binding to calcium. *Biochemistry.* 31:8098–8106.

Klee, C. B. 1977. Conformational transition accompanying the binding of Ca^{2+} to the protein activator of 3′,5′-cyclic adenosine monophosphate phosphodiesterase. *Biochemistry.* 16:1017–1024.

Kraulis, P. J. 1991. MOLSCRIPT: a program to produce both detailed and schematic plots of proteins structures. *J. Appl. Crystallogr.* 24:946–950.

Kung, C., R. R. Preston, M. E. Maley, K.-Y. Ling, J. A. Kanabrocki, B. R. Seavey, and Y. Saimi. 1992. In vivo Paramecium mutants show that calmodulin orchestrates membrane responses to stimuli. *Cell Calcium.* 13:413–425.

Lakowicz, J. R., H. Cherek, B. P. Maliwal, and E. Gratton. 1985. Time-resolved fluorescence anisotropies of diphenylhexatriene and perylene in solvents and lipid bilayers obtained from multifrequency phase-modulation fluorometry. *Biochemistry.* 24:376–383.

Lakowicz, J. R., and I. Gryczynski. 1991. Frequency-domain fluorescence spectroscopy. *In* Topics in Fluorescence Spectroscopy, Vol. I. J. R. Lakowicz, editor. Plenum Press, New York. 293–335.

Ling, V., and R. E. Zielinski. 1989. Cloning of cDNA sequences encoding the calcium-binding protein, calmodulin, from barley (*Hordeum vugare L.*). *Plant Physiol.* 90:714–719.

Luedtke, R., C. S. Owen, J. M. Vanderkooi, and F. Karush. 1981. Proximity relationships within the Fc segment of rabbit immunoglobulin G analyzed by resonance energy transfer. *Biochemistry.* 20:2927–2936.

Lukas, T. J., D. B. Iverson, M. Schleicher, and D. M. Watterson. 1984. Structural characterization of a higher plant calmodulin: *Spinacia oleracea*. *Plant Physiol.* 75:788–795.

MacKall, J., and C. B. Klee. 1991. Calcium-induced sensitization of the central helix of calmodulin to proteolysis. *Biochemistry.* 30:7242–7247.

Maune, J. F., C. B. Klee, and K. Beckingham. 1992. Ca^{2+} binding and conformational change in two series of point mutations to the individual Ca^{2+}-binding sites of calmodulin. *J. Biol. Chem.* 267:5286–5295.

Meador, W. E., A. R. Means, and F. A. Quiocho. 1992. Target enzyme recognition by calmodulin: 2.4 Å structure of a calmodulin-peptide complex. *Science.* 257:1251–1255.

Meador, W. E., A. R. Means, and F. A. Quiocho. 1993. Modulation of calmodulin plasticity in molecular recognition on the basis of X-ray structure. *Science.* 262:1718–1721.

Michaelis, M. L., D. J. Bigelow, Ch. Schöneich, T. D. Williams, L. Ramonda, D. Yin, A. F. R. Hühmer, Y. Yao, J. Gao, and T. C. Squier. 1996. Decreased plasma membrane calcium transport activity in aging brain. *Life Sci.* 59:405–412.

Mukherjea, P., J. F. Maune, and K. Beckingham. 1996. Interlobe communication in multiple calcium-binding site mutants of *Drosophila* calmodulin. *Protein Sci.* 5:468–477.

Murphy, R. C., and K. A. Harrison. 1994. Fast atom bombardment mass spectrometry of phospholipids. *Mass Spectrom. Rev.* 13:57–75.

Nelson, D. P., and L. A. Kiesow. 1972. Enthalpy of decomposition of hydrogen peroxide by catalase at 25 degrees C (with molar extinction coefficients of H_2O_2 in the UV. *Anal. Biochem.* 49:474–478.

Pedigo, S., and M. A. Shea. 1995a. Quantitative endoproteinase GluC footprinting of cooperative Ca^{2+} binding to calmodulin: proteolytic susceptibility of E31 and E87 indicates interdomain interactions. *Biochemistry.* 34:1179–1196.

Pedigo, S., and M. A. Shea. 1995b. Discontinuous equilibrium titrations of cooperative calcium binding to calmodulin by 1-D ^{1}H-nuclear magnetic resonance spectroscopy. *Biochemistry.* 34:10676–10689.

Richardson, J. S., and D. C. Richardson. 1989. Principles and patterns in protein conformation. *In* Prediction of Protein Structure and the Principles of Protein Conformation. G. D. Fasman, editor. Plenum Press, New York. 1–98.

Rosen, D. R., T. Siddeque, D. Patterson, D. A. Figlewicz, P. Sapp, A. Hentati, D. Donaldson, J. Goto, J. P. O'Regan, H.-X. Deng, Z. Rahman, A. Krizus, D. McKenna-Yasek, A. Cayabyab, S. M. Gaston, R. Berger, R. E. Tanzi, J. J. Halperin, B. Herzfeldt, R. Van den Bergh, W.-Y. Hung, T. Bird, G. Deng, D. W. Mudler, C. Smyth, N. G. Laing, E. Sorianao, A. Pericak-Vance, J. Haines, G. A. Rouleau, J. S. Gusella, H. R. Horvitz, and R. H. Brown. 1993. Mutations in Cu/Zn superoxide dismutase gene are associated with familial amyotrophic lateral sclerosis. *Nature.* 362: 59–62.

Royer, C. A. 1993. Understanding fluorescence decays in proteins. *Biophys. J.* 65:9–10.

Sacks, D. B., M. M. Lopez, Z. Li, and D. Kosk-Kosicka. 1996. Analysis of phosphorylation and mutation of tyrosine residues of calmodulin on its activation of the erythrocyte Ca^{2+}-transporting ATPase. *Eur. J. Biochem.* 239:98–104.

Saxena, V. P., and D. B. Wetlaufer. 1971. A new basis for interpreting the circular dichroic spectra of proteins. *Proc. Natl. Acad. Sci. USA.* 66: 969–972.

Sayle, R. A., and E. J. Milner. 1995. RASMOL: biomolecular graphics for all. *Trends Biochem. Sci.* 20:374–376.

Schöneich, Ch., A. F. R. Hühmer, S. R. Rabel, J. F. Stobaugh, S. D. S. Jois, C. K. Larive, T. J. Siahaan, T. C. Squier, D. J. Bigelow, and T. D. Williams. 1995. Separation and analysis of peptides and proteins. *Anal. Chem.* 67:155R–181R.

Seamon, K. B. 1980. Calcium- and magnesium-dependent conformational states of calmodulin as determined by nuclear magnetic resonance. *Biochemistry.* 19:207–215.

Selkoe, D. J. 1997. Alzheimer's disease: genotypes, phenotypes, and treatments. *Science.* 275:630–631.

Shea, M. A., A. S. Verhoeven, and S. Pedigo. 1996. Calcium-induced interactions of calmodulin domains revealed by quantitative thrombin footprinting of Arg^{37} and Arg^{106}. *Biochemistry.* 35:2943–2957.

Small, E. W., and S. R. Anderson. 1988. Fluorescence anisotropy decay demonstrates calcium-dependent shape changes in photo-cross-linked calmodulin. *Biochemistry.* 27:419–428.

Smith, M. A., G. Perry, P. L. Richey, L. M. Sayre, V. W. Anderson, M. F. Beal, and N. Kowall. 1996. Oxidative damage in Alzheimer's. *Nature.* 382:120–121.

Smith, R. D., J. A. Loo, R. R. Ogorzalek, M. Bushman, and H. R. Udseth. 1991. Principles and practice of electrospray ionization-mass spectrometry for large polypeptides and proteins. *Mass. Spectrom. Rev.* 10: 359–451.

Sohal, R. S., and R. Weindruch. 1996. Oxidative stress, caloric restriction, and aging. *Science.* 273:59–63.

Sorensen, B. R., and M. A. Shea. 1996. Calcium binding decreases the Stokes radius of calmodulin and mutants R74A, R90A, and R90G. *Biophys. J.* 71:3407–3420.

Starovasnik, M. A., D.-R. Su, K. Beckingham, and R. E. Klevit. 1992. A series of point mutations reveal interactions between the calcium-binding sites of calmodulin. *Protein Sci.* 1:245–253.

Steiner, R. F. 1991. Fluorescence anisotropy: theory and applications. *In* Topics in Fluorescence Spectroscopy, Vol. 2. J. R. Lakowicz, editor. Plenum Press, New York. 1–52.

Strasburg, G. M., M. Hogan, W. Birmachu, D. D. Thomas, and C. F. Louis. 1988. Site-specific derivatives of wheat germ calmodulin. *J. Biol. Chem.* 263:542–548.

Takezawa, D., Z. H. Liu, G. An, and B. W. Poovaiah. 1995. Calmodulin gene family in potato: developmental and touch-induced expression of the mRNA encoding a novel isoform. *Plant Mol. Biol.* 27:693–703.

Thulin, E., A. Anderson, T. Drakenberg, S. Forsen, and H. J. Vogel. 1984. Metal ion and drug binding to proteolytic fragments of calmodulin: proteolytic, cadmium-113, and proton nuclear magnetic resonance studies. *Biochemistry.* 23:1862–1870.

Toda, H., M. Yazawa, F. Sakiyama, and K. Yagi. 1985. Amino acid sequence of calmodulin from wheat germ. *J. Biochem. (Tokyo).* 98: 833–842.

Toda, H., M. Yazawa, F. Sakiyama, and K. Yagi. 1994. Correction to amino acid sequence of calmodulin from wheat germ. *J. Biochem. (Tokyo).* 115:367.

Török, K., A. N. Lane, S. N. Martin, J.-M. Janot, and P. M. Bailey. 1992. Effects of calcium binding on the internal dynamic properties of bovine brain calmodulin, studied by NMR and optical spectroscopy. *Biochemistry.* 31:3452–3462.

Wang, C.-L. A., P. C. Leavis, and J. Gergely. 1984. Kinetic studies show that Ca^{2+} and Tb^{3+} have different binding preferences toward the four Ca^{2+} binding sites of calmodulin. *Biochemistry.* 23:6410–6415.

Weber, G. 1981. Resolution of the fluorescence lifetimes in a heterogeneous system by phase and modulation measurements. *J. Phys. Chem.* 85:949–953.

Yang, T., G. Segal, S. Abbo, M. Feldman, and H. Fromm. 1996. Characterization of the calmodulin gene family in wheat: structure, chromosomal location, and evolutionary aspects. *Mol. Gen. Genet.* 252: 684–694.

Yao, Y., Ch. Schöneich, and T. C. Squier. 1994. Resolution of structural changes associated with calcium activation of calmodulin using frequency-domain fluorescence spectroscopy. *Biochemistry.* 33: 7797–7810.

Yao, Y., and T. C. Squier. 1996. Variable conformation and dynamics of calmodulin complexed with peptides derived from the autoinhibitory domains of target proteins. *Biochemistry.* 35:6815–6827.

Yao, Y., D. Yin, G. Jas, K. Kuczera, T. D. Williams, Ch. Schöneich, and T. C. Squier. 1996. Oxidative modification of a carboxyl-terminal methionine in calmodulin by hydrogen peroxide inhibits calmodulin-dependent activation of the plasma membrane Ca-ATPase. *Biochemistry.* 35:2767–2787.

Yin, D., A. Hühmer, Ch. Schöneich, and T. C. Squier. 1995. Vicinal methionines define the oxidatively sensitive sites on calmodulin. *Biophys. J.* 68:A165.

Yoshida, M., O. Minowa, and K. Yagi. 1983. Divalent cation binding to wheat germ calmodulin. *J. Biochem. (Tokyo).* 94:1925–1933.

Zhang, M., M. Li, J. H. Wang, and H. J. Vogel. 1994. The effect of Met → Leu mutations on calmodulin's ability to activate cyclic nucleotide phosphodiesterase. *J. Biol. Chem.* 269:15546–15552.

Zhang, M., T. Tanaka, and M. Ikura. 1995. Calcium-induced conformational transition revealed by the solution structure of apo calmodulin. *Nature Struct. Biol.* 2:758–767.